Transportation Consortium of South-Central States

Solving Emerging Transportation Resiliency, Sustainability, and Economic Challenges through the Use of Innovative Materials and Construction Methods: From Research to Implementation

Development of Corrosion Inhibiting Geopolymers Based Cement for Transportation Infrastructure

Project No. 19CTAM02

Lead University: Texas A&M University

Final Report

November 2020

Disclaimer

The contents of this report reflect the views of the authors, who are responsible for the facts and the accuracy of the information presented herein. This document is disseminated in the interest of information exchange. The report is funded, partially or entirely, by a grant from the U.S. Department of Transportation's University Transportation Centers Program. However, the U.S. Government assumes no liability for the contents or use thereof.

Acknowledgements

The authors would like to acknowledge the financial support for this study by the Transportation Consortium of South-Central States (Tran-SET). Furthermore, the authors would like to acknowledge the support of BASF for providing materials used in the study.

TECHNICAL DOCUMENTATION PAGE

1. Project No.	2. Government Accession No.	3. Recipient's Catalog No.
19CTAM02		

4. Title and Subtitle	5. Report Date
Development of Corrosion Inhibiting Geopolymers Based Cement for Transportation Infrastructure	Nov. 2020
	6. Performing Organization Code
7. Author(s)	**8. Performing Organization Report No.**
PI: Homero Castaneda-Lopez https://orcid.org/0000-0002-9252-7744 Co-PI: Miladin Radovic https://orcid.org/0000-0003-4571-2848 GRA: Changkyu Kim https://orcid.org/0000-0002-9050-6309 GRA: Oscar Huang https://orcid.org/0000-0001-7004-3506	
9. Performing Organization Name and Address	**10. Work Unit No. (TRAIS)**
Transportation Consortium of South-Central States (Tran-SET) University Transportation Center for Region 6 3319 Patrick F. Taylor Hall, Louisiana State University, Baton Rouge, LA 70803	**11. Contract or Grant No.** 69A3551747106
12. Sponsoring Agency Name and Address	**13. Type of Report and Period Covered**
United States of America Department of Transportation Research and Innovative Technology Administration	Final Research Report Aug. 2019 – Nov. 2020
	14. Sponsoring Agency Code

15. Supplementary Notes

Report uploaded and accessible at Tran-SET's website (http://transet.lsu.edu/).

16. Abstract

Geopolymers are gaining attention as affordable, sustainable, and eco-friendly replacement for Ordinary Portland Cement (OPC) in concrete civil structures. More importantly, Geopolymer-based Cement (GPC) provide sustainable and environmentally friendly alternative to OPCs as GPC can be processed at room temperatures from aqueous solutions of waste materials (e.g., fly ash) or abounded natural sources (e.g., clay) and thus reduce significant CO_2 production associated with processing of OPC. Although, a lot of work has been done on improving mechanical properties of GPC over the last two decades, there are only a few studies on effects of GPC concrete on steel rebar reinforcement. Even though all those studies indicate that GPC inhibits corrosion of reinforcing streel when compared to OPC, the inhibition mechanism is still unclear and geopolymer composition is yet to be optimized to achieve the best inhibition properties. A collaborative research study is formulated by a team from TAMU to investigate the long-term durability of reinforced GPC concrete against chloride-induced corrosion. Various parameters of GPC such as Si/Al, water/solids, alkali ion/Al ratios would affect various structural and mechanical properties of GPC. Therefore, GPCs will need to be studied thoroughly in order to optimize the use of local waste and natural materials for transportation infrastructure in Region 6. As a part of the proposed study, durability tests under simulated marine environment are to be conducted on reinforced GPC concrete over long periods of time. Both material characterization studies related to micro to macro behavioral changes during long-term exposure of reinforced GPC concrete and steel rebar will be carried out as a part of this research.

17. Key Words	18. Distribution Statement
Geopolymer, Reinforced Concrete, Corrosion	No restrictions. This document is available through the National Technical Information Service, Springfield, VA 22161.

19. Security Classif. (of this report)	20. Security Classif. (of this page)	21. No. of Pages	22. Price
Unclassified	Unclassified	34	

Form DOT F 1700.7 (8-72) **Reproduction of completed page authorized.**

SI* (MODERN METRIC) CONVERSION FACTORS

APPROXIMATE CONVERSIONS TO SI UNITS

Symbol	When You Know	Multiply By	To Find	Symbol
		LENGTH		
in	inches	25.4	millimeters	mm
ft	feet	0.305	meters	m
yd	yards	0.914	meters	m
mi	miles	1.61	kilometers	km
		AREA		
in^2	square inches	645.2	square millimeters	mm^2
ft^2	square feet	0.093	square meters	m^2
yd^2	square yard	0.836	square meters	m^2
ac	acres	0.405	hectares	ha
mi^2	square miles	2.59	square kilometers	km^2
		VOLUME		
fl oz	fluid ounces	29.57	milliliters	mL
gal	gallons	3.785	liters	L
ft^3	cubic feet	0.028	cubic meters	m^3
yd^3	cubic yards	0.765	cubic meters	m^3
		NOTE: volumes greater than 1000 L shall be shown in m^3		
		MASS		
oz	ounces	28.35	grams	g
lb	pounds	0.454	kilograms	kg
T	short tons (2000 lb)	0.907	megagrams (or "metric ton")	Mg (or "t")
		TEMPERATURE (exact degrees)		
°F	Fahrenheit	5 (F-32)/9 or (F-32)/1.8	Celsius	°C
		ILLUMINATION		
fc	foot-candles	10.76	lux	lx
fl	foot-Lamberts	3.426	$candela/m^2$	cd/m^2
		FORCE and PRESSURE or STRESS		
lbf	poundforce	4.45	newtons	N
lbf/in^2	poundforce per square inch	6.89	kilopascals	kPa

APPROXIMATE CONVERSIONS FROM SI UNITS

Symbol	When You Know	Multiply By	To Find	Symbol
		LENGTH		
mm	millimeters	0.039	inches	in
m	meters	3.28	feet	ft
m	meters	1.09	yards	yd
km	kilometers	0.621	miles	mi
		AREA		
mm^2	square millimeters	0.0016	square inches	in^2
m	square meters	10.764	square feet	ft^2
m	square meters	1.195	square yards	yd^2
ha	hectares	2.47	acres	ac
km	square kilometers	0.386	square miles	mi^2
		VOLUME		
mL	milliliters	0.034	fluid ounces	fl oz
L	liters	0.264	gallons	gal
m	cubic meters	35.314	cubic feet	ft^3
m	cubic meters	1.307	cubic yards	yd^3
		MASS		
g	grams	0.035	ounces	oz
kg	kilograms	2.202	pounds	lb
Mg (or "t")	megagrams (or "metric ton")	1.103	short tons (2000 lb)	T
		TEMPERATURE (exact degrees)		
C	Celsius	1.8C+32	Fahrenheit	°F
		ILLUMINATION		
lx	lux	0.0929	foot-candles	fc
cd/m^2	$candela/m^2$	0.2919	foot-Lamberts	fl
		FORCE and PRESSURE or STRESS		
N	newtons	0.225	poundforce	lbf
kPa	kilopascals	0.145	poundforce per square inch	lbf/in^2

TABLE OF CONTENTS

LIST OF FIGURES

LIST OF TABLES

ACRONYMS, ABBREVIATIONS, AND SYMBOLS

Al	Aluminum
C_{be}	Bulk-Electrode Capacitance
C_c	Concrete Bulk Pore Capacitance
C_{dl}	Double-Layer Capacitance
CE	Counter Electrode
Cl	Chlorine/Chloride ion
CPE	Constant Phase Element
EC	Equivalent Circuit
EDS	Energy-Dispersive X-Ray Spectroscopy
EIS	Electrochemical Impedance Spectroscopy
FA	Fly Ash
GPs	Geopolymers
K	Potassium
K-GP	Potassium-based Geopolymer
MK	Metakaolin
Na	Sodium
Na-GP	Sodium-based Geopolymer
NaCl	Sodium Chloride
NMR	Nuclear Magnetic Resonance
OCP	Open Circuit Potential
OM	Optical Microscopy
OPC	Ordinary Portland Cement
R_{be}	Bulk-Electrode Resistance
R_c	Concrete Bulk Resistance
R_{ct}	Charge-Transfer Resistance
R_s	Solution Resistance
RC	Reinforced Concrete
RE	Reference Electrode
RPM	Revolution Per Minute

SCE	Saturated Calomel Electrode
SEM	Scanning Electron Microscopy
Si	Silicon
WE	Working Electrode
XRD	X-Ray Diffraction

EXECUTIVE SUMMARY

In order to improve the durability of the transportation infrastructure affected by corrosion in the most efficient manner, we proposed to characterize and develop a new material to manage corrosion in reinforced concrete (RC) elements. The desirable features of this propose material system would include the barrier effect to the corrosion precursors and harsh environment hindering the RC elements with time.

The proposed study for the geopolymer based cements (GPC) show good mechanical and chemical results for some mixtures and the corrosion resistance properties, as it provides new approach for eco-friendly components. The current research with reinforced GPC concrete, provides sustainable greener alternative for the existing reinforced concrete infrastructure and a potential to have one or two control mechanisms for corrosion control (barrier and inhibition effect) in durable system. The methodology developed was optimized following new processing routes, the physical properties and electrochemical results are pointing in the direction to improve the RC systems. The equivalent circuit analogs characterized quantitatively the parameters for the GPC system prone to have more durability.

Based on the experimental findings, GPC showed better corrosion inhibiting performance when it is sodium-based, the $SiO_2 = 3$ instead of 4, lower water/solids ratio, and higher alkali/aluminum ratio. Out of all the parameter, the alkali cation seems to have the most impact on the corrosion inhibiting performance. Optical microscopy showed that the rebar and GPC still form a good interface even after electrochemical tests indicating severe corrosion in the rebar.

The analysis included deterministic modeling in order to characterize the mechanisms occurring at the interface rebar-geopolymer system, the experimental data available permitted to quantitatively characterize the geopolymer system without considering the probabilistic approach. The electrochemical parameters based on the equivalent circuit analysis were able to characterize and quantify the performance of the different compositions proposed in the geopolymer based material.

The expected deliverable from this project is a technical report summarizing all tasks and findings including necessary design guidelines of durable reinforced GPC concrete structures. The team also anticipates publishing high-impact research publications including journal and conference articles.

1. INTRODUCTION

Reinforced concrete (RC) is a ubiquitous choice of material for transportation infrastructure due to its low-cost, high compressive strength, and ease of use. The most common combination usually is ordinary Portland cement (OPC) binder with steel rebar. Since OPC creates a highly alkaline environment (pH > 12), the steel rebar is able to form a passive layer to minimize the corrosion rate and prolong the its integrity (*1*). However, there are various common aggressive agents (e.g., chloride ions, sulfate ions) that can breakdown the passive layer and/or reduce the pH of OPC, which then causes corrosion in the steel rebar. The formation of the corrosion product would then induce tensile stresses in the concrete and further compromises the integrity of the structure through cracking and delamination (*2*). To counteract this problem, various approaches have been taken to prolong the durability of RC. One of these approaches is to modify the rebar with coatings acting as either a dense barrier (e.g., epoxy) (*3*) or a sacrificial barrier (galvanize with Zn) (*4; 5*) to further reduce the rate for the aggressive agents to reach the steel. Another common approach is to add corrosion inhibiting agents such as calcium nitrate into the cement mix to slow down the diffusion rate of the aggressive agents (*2*). All of these methods have proven to be effective to a certain degree, however, corrosion is a persisting problem with steel and researchers are always looking for more effective and innovative ways to prolong its service life.

Another issue with OPC is its impact on the environment during the production process. OPC is the most produced man-made material (3.5 billion tones in 2015), and it is estimated that 5-6% of the anthropological CO_2 emission is due to OPC production (*6*). The production of OPC is an energy-intensive process that requires high temperature for the clay and calcium carbonate to react, in addition, the reaction also releases a large amount of CO_2 (*7*). Recently, a new class of aluminosilicate polymers known as geopolymers (GPs) have received much attention as an eco-friendly and sustainable alternative to OPC in various transportation infrastructure applications (*8*). Geopolymer-based cement (GPC) is a family of materials that consists of three-dimensional non-crystalline aluminosilicates network stabilized with alkali cations (*9*). The main attraction with GPC is that it can be processed with waste materials (e.g., fly ash, steel slag) and/or natural resources (e.g., calcined clay), which are inexpensive and abundant, at room temperature while still have properties such as compressive strength similar to that of OPC (*10-12*). More importantly, studies have shown that the use of GPC can reduce CO_2 emission up to 44-64% when compared to the use of OPC (*13*).

This report covers the work on the durability of reinforced GPC concrete when exposed to simulated corrosive marine environment. This would provide an insight to the applicability of this new class of sustainable and eco-friendly material for the transportation infrastructure in the coastal area of Region 6.

2. OBJECTIVES

The overall objective of this project is to develop an innovative, sustainable, eco-friendly, and durable GPC for reinforced concrete infrastructure in Region 6, using natural and waste materials that are abundant in the region. This research should bring major benefits in the design of durable infrastructure in problematic conditions that prevail Region 6.

More specific objectives of the proposed projects are:

- Conduct electrochemical testing of GPC concrete reinforced with steel rebar in simulated corrosive marine environment using both AC and DC methods;
- Determine corrosion mechanism and kinetics of the reinforcement steel in GPC concrete;
- Optimize GPC composition for maximum corrosion protection of reinforcing steel rebar;
- Provide guidance for the industry on optimizing GPC composition for maximum corrosion protection and disseminate that guidance to the industry of interest; and
- Develop corrosion management system that would include the methods for preliminary corrosion condition evaluation and in-depth corrosion condition evaluation, the methods for assessing the structure condition rating and monitoring, methodology for selecting best corrosion prevention and controls, reliability model, and procedure for tracking repair or design performance in GPCs.

3. LITERATURE REVIEW

3.1. Geopolymers

Geopolymers (GPs) are a class of amorphous inorganic aluminosilicates that is charged balanced by alkali metal cations. Since its first development by Joseph Davidovits in the 1970s (*14; 15*), GPs have been studied for numerous applications such as thermal insulating and fire-resistant coating (*16*), encapsulation of radioactive waste (*17*), water purification filter (*18*) , and most extensively as cementitious material alternative to OPC (*8*). The chemistry of GPs can be describe with the formula $M_n[-(SiO_2)_z-AlO_2-]\cdot wH_2O$ where M is the alkali metal cation (usually Na^+ or K^+), n is the degree of polymerization or molar ratio of M/Al, z is the molar ratio of Si/Al, and w is the molar water quantity. It is worth noting that GPs are usually prepared with a Si/Al ratio of 1.8-2.2, a $H_2O/(Al_2O_3+SiO_2)$ ratio of 2.0-5.0, and a M/Al ratio of 0.9-1.2 (*9*). GPC has been most extensively studied as an alternative to OPC because it can be processed from waste material (e.g. fly ash, steel slag) (*10; 11*) and natural material (e.g. calcine clay, rice husk ash, volcanic ash) (*19-21*) at near ambient condition while having a much lower carbon footprint. All of the precursor materials for the synthesis of GP are rich in aluminosilicate that dissolves into $[(SiO)OH_3]^-$, $[(SiO_2)OH_2]^{2-}$, $[(AlO)OH_4]^-$ etc. The synthesis of GPC starts with dissolving the aluminosilicate precursor in highly alkaline aqueous solution of NaOH and/or KOH. The Si/Al ratio can be adjusted with soluble silica such as silica fume and alkali (sodium or potassium) silicate. Upon mixing, aluminosilicate precursor dissociates into monomeric and oligomeric species of Si and Al through hydrolysis. As GP cures, the Si and Al species begin to chain together forming -Al-O-Si- and -Si-O-Si bonds through polycondensation process, in which the gel becomes more rigid with the curing time and excess water is released. The chains will continue to grow and crosslink until an amorphous rigid gel with three-dimensional structure is formed (*9; 22*). The final structure of GP can be described as an inorganic polymer with $[SiO_4]^{4-}$ and $[AlO_4]^{5-}$ tetrahedra monomeric units in IV-fold coordination, where the IV-coordinated aluminum is unique to GPC and distinct it from other aluminosilicate materials with similar chemistry (*23*). The alkali cations are theorized to charge balance the negatively charged aluminum in the structure while retaining some of the water even after GPC has fully cured (*24; 25*).

GPC represents a complex class of materials that has many factors to influence its properties such as source of aluminosilicate, Si/Al ratio, water/solids ratio used during processing, alkali/aluminum ratio, mixing and curing condition, etc. While it may seem overwhelming to optimize all parameters for an application, GPC has been extensively studied over the past decades and summarized elsewhere (*8; 22; 26*). To summarize some of the critical findings on each of the parameters, the source of aluminosilicate can heavily influence the fresh properties and rate of curing due to the availability of aluminum (*27*). For example, the use of metakaolin (MK) can result in a thicker paste but have an earlier strength development due to the readily available reactive phases of aluminum, while fly ash (FA) would result in a more workable paste with the same water content but would require a longer time to set and cure. It is also established that higher Si/Al ratio up to 2 usually result in better properties such as mechanical strength since it -Si-O-Si- bond is stronger than -Al-O-Si and allows a more complex interconnected network (*19; 28*). Similar to OPC, GPC is very sensitive to the water content used during processing. Higher water content result in a more workable fresh paste but would take a longer time to set and cure, and result in a more porous network that is lower in density and lower in mechanical properties (*25*). By increasing the alkali/Al ratio, the excess alkali cations are theorized to act as a “chain

terminator" during the polycondensation process. In other words, higher alkali/Al ratio prevents the chains from fully developed resulting in a less complex network. In addition, alkali cation can chemically bond with water making the GPC more hydrophilic (*9; 25*). Overall, GP is a versatile class of material that has many chemical and processing parameters with many niche applications. However, instead of having a single optimal composition for all the applications, GP can be optimized depending on the need of the application.

3.2. Geopolymer-based Cement Concrete

Geopolymer concrete (GPC) has been of interest since the early 2000s and achieved strength that is on par with OPC concrete (*12; 29; 30*). However, as of 2016, most of the studies focuses on optimizing FA-based GPC concrete while curing them under elevated temperature, which is not ideal for implementation (*8*). The main shortcoming with studies that utilize FA is that FA does not have a consistent composition and it can vary a lot depending on the location that it is sourced from. This means that it is usually difficult to reproduce the studies, in addition, the price of FA has been surging lately with the increase in demand from the concrete industry and the shift of energy production from coal plants. MK-based GPC has been more extensively studied in the past few decades for a more fundamental understanding on GPC since it is a pure aluminosilicate source that is reactive and more consistent regardless of the source. Some of the examples are physical evolution with temperature (*31-33*), formation of crystalline phase (*34; 35*), structural studies using nuclear magnetic resonance (NMR) spectroscopy (*23*). However, there are only a few studies on mechanical properties and long-term durability (*28; 36-41*). One of the main issues with the durability of concrete structure is the corrosion of steel rebar reinforcement, which is an extensive field of interest in the OPC community (*1*), but not a lot of research has been done for reinforced GPC concrete. Many researchers have claimed GPC to be better than OPC when it comes to inhibiting corrosion (*9; 26*), however, there are only about half a dozen of papers available in the public domain, and they have conflicting conclusions on the corrosion inhibiting performance of GPC (*42-48*). One of the main reasons for the conflicting results is because all of the research except for part of one use FA, and as mentioned before, FA can produce different results due to varied composition from different sources. Another issue that makes it difficult to compare between the studies is that all the conclusions were drawn without any sort of systematic parametric testing, in order words, none of the studies provide any guidance towards producing better GP to inhibit rebar corrosion. Instead, the studies synthesized a couple of GP compositions and draws the conclusion from there. The rest of the section will do an in-depth review on the available literature that investigated the chloride-induced corrosion inhibiting performance of GPC in chronological order.

Miranda et al. (*42*) is one of the earliest study on the chloride-induced corrosion resistant performance of GPC. Miranda et al. compared OPC mortar with two types of FA-based GPC mortars where one was activated with sodium hydroxide while the other was activated with a mixture of sodium hydroxide and sodium silicate. The samples were cured in elevated temperature and designed in a way that there's a 7 mm penetration depth between the surface and the steel rebar, but the detailed condition on the corrosive environment were not reported in the paper. Through electrochemical measurements, it was shown in the study that FA-based GPC achieves a better early protection than OPC, but the degree of protection decreases gradually for FA-based GPC while it improves for OPC during the 3-month testing period. This is most likely because fresh GPC paste already has a high pH because of the activating solution, while OPC becomes more alkaline with time as more and more of the components dissolve. Overall, this study showed

that FA-based GPC is not as effective as OPC to protect steel rebar from chloride-induced corrosion in the long term.

Reddy et al. (*43*) compared OPC concrete with two types of FA-based GPC concrete, where one was synthesized with 8M sodium hydroxide-sodium silicate blend while the other was synthesized with 14M sodium hydroxide-sodium silicate blend. The OPC concrete specimens were cured in ambient condition while the GPC concrete specimens were cured in elevated condition. The specimens partially immersed in seawater solution for 21 days before testing, then a DC current is applied to accelerate the corrosion. This study clearly showed that GPC concrete is vastly superior over OPC concrete with corrosion current measurement and weight loss measurement of the rebar. Particularly for the weight loss measurement of rebar, the 3 rebars in OPC loss between 50-75% of the weight while all 6 rebars in GPC showed no significant weight loss. Even though GPC showed significantly better performance over OPC, the result should still be taken with a grain of salt since GPC specimens are cured under elevated conditions while OPC specimens weren't. Another factor that could have affected the study is the difference in water content and superplasticizer between GPC and OPC specimens since the GPC specimens had superplasticizer and significantly less water than the OPC specimens.

In Shaikh's work (*44*), 7 mixes were made with OPC as the control mix and the rest are GPC with either 14M or 16M NaOH and ratio of sodium silicate to sodium hydroxide between 2.5-3.5. The samples were made so that there is a 42 mm of penetration depth from the surface to the rebar. The concrete samples were subjected to 8 wet/dry cycles with 4 days in 3.5 wt% sodium chloride solution and 3 days of drying. Shaikh reported that GPC samples overall performed better than OPC samples in terms of rebar mass loss, chloride penetration, and open-circuit potential (OCP). From the mass loss measurement, it was observed that OPC did not have good adhesion to rebar while GPC did, and the rebars in OPC loss about 0.5% of mass while no significant mass loss can be measured from rebars in GPC samples. It was also observed from chloride penetration and OCP test that GPC with higher concentrated sodium hydroxide and more sodium silicate performed better. A potential explanation for these results is that the more concentrated sodium hydroxide solution is able to dissolve the FA better and higher content of sodium silicate provides more dissolved silica for geopolymerization.

Chindaprasirt et al. (*45*) prepared 6 different mixes of GPC using varied concentration of sodium hydroxide ranging from 8 to 18M with class C FA. The samples were made so that there's a 94 mm of penetration depth between the surface and the rebar. The samples are cured for 28 days in ambient condition and then exposed to marine environment for 3 years. The study shows that the FA-based GPC can effectively inhibit the diffusion of chloride ions when the activator solution (sodium hydroxide) is more than 14M. The weight loss measurement of rebar also observes the same result from the chloride diffusion test. This study showed that class C FA-based GPC concrete in real marine environment has some promising potentials, however, it did not show how OPC would perform under the same condition. In addition, the parametric test done in this study simply showed that well-reacted GPC can inhibit the diffusion of chloride better and does not provide any further insights.

Babaee et al. (*46*) investigated the performance of 1 GPC composition using a blend of FA, ultra-fine FA, and ground granulated blast-furnace slag activated by a mixture of 12M sodium hydroxide and sodium silicate. The samples are made so that there's a penetration depth of 73 mm, and then cured under elevated temperature. For testing, the samples are subjected to 1 week of immersion

in 3.5 wt% sodium chloride solution, then exposed to ambient condition for 2 weeks for a total of 11 cycles. From OCP and linear polarization resistance measurements, it was found that the GPC samples has comparable performance with the results on OPC from one of their previous studies (*49*). This study has done a very thorough investigation on the chloride-induced corrosion performance of GPC, the only shortcoming would be the lack parametric study and the usage of local materials, which does not give much guidance to other researchers who would want to further the study.

Tennakoon et al. (*47*) compared OPC with 3 different mixes of GPC that used different FA to slag ratios. The FA and slag are activated with sodium silicate, and the samples are cured in ambient condition for 28 days. The samples were prepared so that there's a penetration depth of 465 mm, and then they were immersed in either 2.83M (16.5 wt%) or 0.6M (3.5 wt%) NaCl solutions. From OCP measurements alone, GPC seems to be inferior when compared to OPC, however, GPC showed better results when looking chloride penetration and visual inspection of the corrosion product on the rebar. Between the 3 GPC compositions, the composition with more slag outperforms the ones with less slag. Overall, this study showed some very interesting results, and the disconnect between electrochemical results and corrosion activity would need further investigations.

Gunasekara et al. (*48*) compared OPC with GPC made from 3 different FAs. The FAs were activated with a mixture of 15M sodium hydroxide and sodium silicate. The samples were made so that there's a 70 mm penetration depth and then cured in elevated temperature condition. After curing, the samples are exposed to 3% sodium chloride solution for a week then ambient condition for 2 weeks, and the cycled for 540 days. Overall, GPC shows similar performance compared to OPC unless chloride is added into the concrete mix, then in that case OPC outperforms GPC significantly. This study also showed that different FA can have significantly varied performance, depending on its composition and reactivity.

4. METHODOLOGY

4.1. Geopolymer Synthesis

The GPs used in this research were synthesized by researchers using sodium or potassium hydroxide (Noah Technologies, TX), amorphous fumed silicon (IV) oxide (Alfa Aesar, MA) with 350- 410 m^2/g specific surface area, MetaMax® (BASF Catalysts LLC, NJ) metakaolin, and deionized water. Metakaolin is a purer aluminosilicate source than the more commonly used fly ash with higher impurities and was therefore used as a precursor for GP synthesis in this research.

The sodium or potassium hydroxide was dissolved in deionized water to create a highly alkaline solution to process the alkali metal cations. The amorphous fumed silicon oxide was then added to adjust the SiO_2/Al_2O_3 ratio of the final product as desired, to create the activating solution for the synthesis of geopolymer. The activating solution was then mixed with metakaolin, which is a high-purity activating aluminosilicate source in a high-sheared mixer for 6 minutes at 400 revolutions per minute (RPM) to create a homogenized mixture, known as GP.

4.2. Selection of Geopolymer Compositions

Since GPC has 4 chemical parameters, the number of possible compositions is endless and was narrowed down to a few compositions, while still having enough variation to efficiently test the effect for each of the parameters. Based on the work done within Tran-SET project #19CLSU04, several preliminary compositions were chosen because of their good compressive strengths, then the compositions were adjusted so that there are enough number of tests done on each of the 4 parameters. The study was separated into 2 phases – during the first phase, 10 compositions were cured for 14 days, then during the second phase, the compositions were narrowed down to 4 based on the results from the first phase for further testing after curing for 28 days. Note that all GPC samples with different compositions are labeled as KXYZ or NaXYZ, where the first letters denote potassium (K) or sodium (Na) while XYZ numbers denote SiO_2/Al_2O_3 ratio, water to solid ratio used to prepare GPC, and Na/Al or K/Al ratio respectively. For example, GPC sample K421 is sample prepared with K-activator, and SiO_2/Al_2O_3=4, water/solid ratio=2, and K/Al=1. The compositions can be found in Table 1.

Table 1. List of GP Compositions.

Test Set	K-GP	Na-GP
Set 1	K 3(2.5)1	Na 331
	K 331	Na 3(3.5)1
	K 33(1.2)	Na 3(3.5)(1.2)
	K 431	Na 431
	K 431	Na 43(1.2)
Set 2	K 3(2.5)(1.2)	Na 331
	K 33(1.2)	Na 3(3.5)(1.2)

4.3. Preparation of Reinforced Geopolymer-based Cement Concrete Specimen

4.3.1. Mix Design of Geopolymer-based Cement Concrete

In order to produce a fresh concrete paste with minimal porosity in the hardened concrete, several test mixes were made with OPC as shown in Table 2. The test mixes were made with TXI Type I/II Portland Cement (TXI, TX) purchased from Home Depot, 5/8" and 3/8" pea gravel from local vendor (All American Stone & Turf, TX), and ASTM C778 (*50*) graded sand from Humboldt (Humboldt Mfg. Co., IL). To make the test mixes, dried cement powder and air-dried aggregates were measured out and mixed together manually in a metal bowl. Then deionized water was added in portion to make sure the mix was evenly hydrated. The concrete mix was then poured into a 2" x 4" cylindrical mold in 2 layers, then cured under sealed condition for 7 days. After 7 days, the OPC concrete specimens were demolded and inspected visually.

Table 2. Test Mix Designs.

Mixture Number	Cement : Coarse Aggregate : Sand : Water Ratio (in mass)
1	1 : 1.5 : 2 : 0.5
2	1 : 1.5 : 3 : 0.5
3	1 : 2 : 3 : 0.5
4	1 : 3 : 3 : 0.5

The cement to aggregate ratio from mixture number 1 was chosen as the most optimal mix and used for the rest of the study with GPC as binder. For the preparation of reinforced GPC concrete, 4" x 4" x 18" molds were used where plastic-wrapped wooden plates were inserted to section off the mold into 2 4-inch cubes. Each of the wooden plates were also drilled to have holes for the rebar to be place in the center of the cube. To make the GPC concrete mix, air-dried aggregates were measured out and mixed manually in a metal bowl. Then fresh GPC paste is prepared in accordance to section 4.1. Geopolymer Synthesis, then added into the aggregate mix. After the GPC concrete mix has become homogeneous, it was poured into the mold in 2 layers, then vacuumed to remove the air bubbles from the concrete. All compositions were made with 2 duplicates for the immersion test (i.e., there are 2 identical samples for each of the compositions). The set 1 test specimens were cured in Ziploc bags for 7 days, then demolded and cured in ambient laboratory condition for another 7-day resulting in a total curing time of 14 days. Set 2 test specimens were cured in Ziploc bags for 7 days, then demolded and put back into the Ziploc bags for another 14 days. Then they were removed from the bag and left to cure in ambient laboratory condition for 7 days for a total of 28 days. Since set 1 testing showed that there's no significant difference in the electrochemical results between the duplicates for most of the compositions, a thin layer of epoxy was applied onto the surfaces of 1 sample for each of the compositions in set 2 on the 27^{th} day to investigate the effect. For fog chamber test, 1 additional sample is made for compositions from set 2 and cured for 14 days similar to the curing regime of set 1 samples. The fog chamber samples are coated with a thin layer of epoxy across all surfaces except for the testing area.

4.3.2. Preparation of Corrosion Testing Specimens

To properly perform the immersion testing of the concrete specimens, the specimens were mounted with dam to contain the electrolyte as shown in Figure 1. The mounting of the dam was performed after the curing process. The specification of the dam area was 2" x 2" mounted with epoxy resin. The mounted dam was filled with 200 mL 3.5 wt.% NaCl electrolyte to simulate the sea water condition.

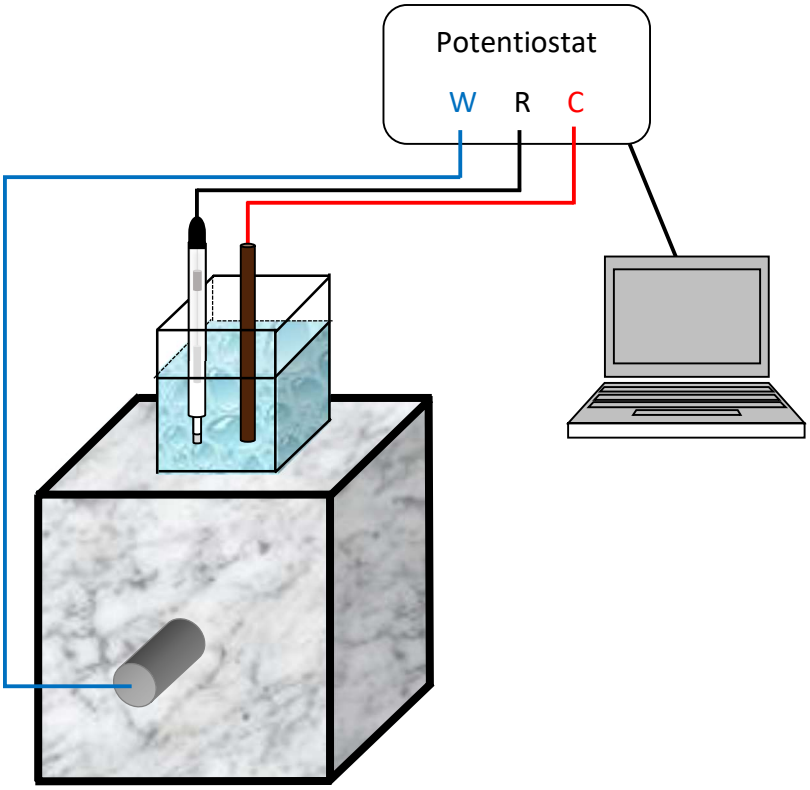

Figure 1. Schematics of Electrochemical Testing.

4.4. Electrochemical Corrosion Testing

4.4.1. Immersion Test

The performance of the produced GPC samples was characterized by electrochemical impedance spectroscopy (EIS) at room temperature with applied electrolyte. The EIS is a powerful non-destructive technique that allows the user to monitor, characterize, and determine the performance of the RC system and efficiency in different environments (*51-53*). A large number of corrosion results under immersed concrete tests have been analyzed on visual inspection, which is dependent on one's individual viewpoint and could not be explained quantitatively (*5; 54; 55*). To overcome the qualitative weakness of visual inspection EIS is utilized to quantitatively monitor the electrochemical processes of the system while it is under constant immersion condition.

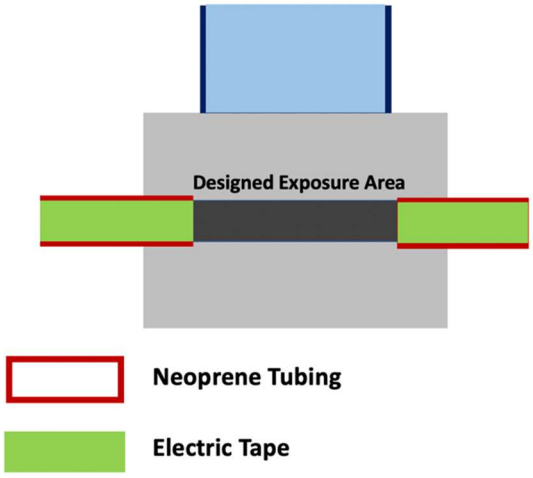

Figure 2. Cross-sectional schematic for electrochemical testing with designed exposure area.

The constant immersion testing was performed using the aforementioned dam filled with 200 mL of 3.5 wt% NaCl electrolyte with an exposed area of 24.55 cm^2 using the Gamry 1000E Potentiostat/Galvanostat. The rebar substrates which were samples of interest, were used as the working electrodes (WE), while graphite rod which was an inert electrode was used for passage of current worked as a counter electrode (CE). A saturated calomel electrode (SCE) was used as a reference electrode (RE) to measure the potential, as shown in Figure 3. The test sequence involved 20 minute of open circuit potential (OCP) followed by EIS at frequencies of 100 kHz to 0.03 Hz with 10 points per decade and an amplitude of 10 mV rms.

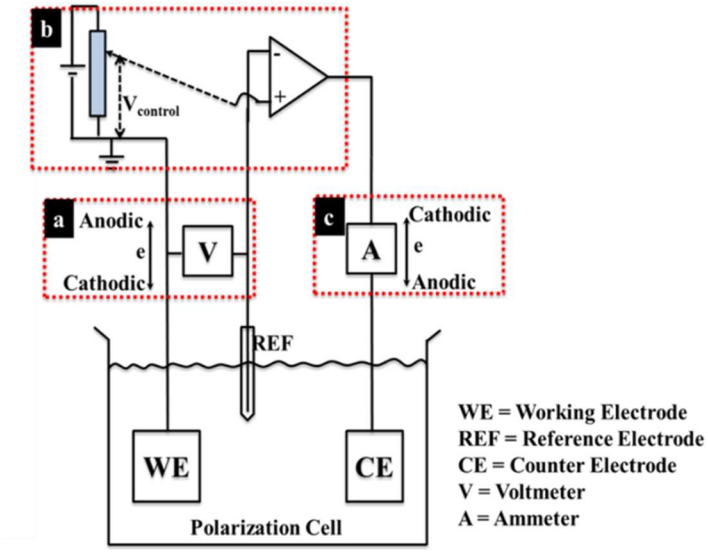

Figure 3. The Three-Electrode System.

4.4.2. Fog Chamber Testing

In addition to the immersion test with the dam, the sample with relatively better performance of each cation-based GPCs were chosen to test under more aggressive conditions. From the K-based GPCs, K3(2.5)(1.2) and K33(1.2) were chosen, meanwhile the Na3(3.5)(1.2) and Na43(1.2) were

chosen from the Na-based GPCs according to the phase 1 results. The fog chamber testing followed a continued wet cycle to examine corrosion behavior more in an accelerated manner. To prevent water uptake from all around the concrete sample, the sample was thoroughly coated with epoxy except the entrance spot that limits the water entering direction to allow more simplified water-uptake scenario. The design of sample preparation is shown in Figure 4.

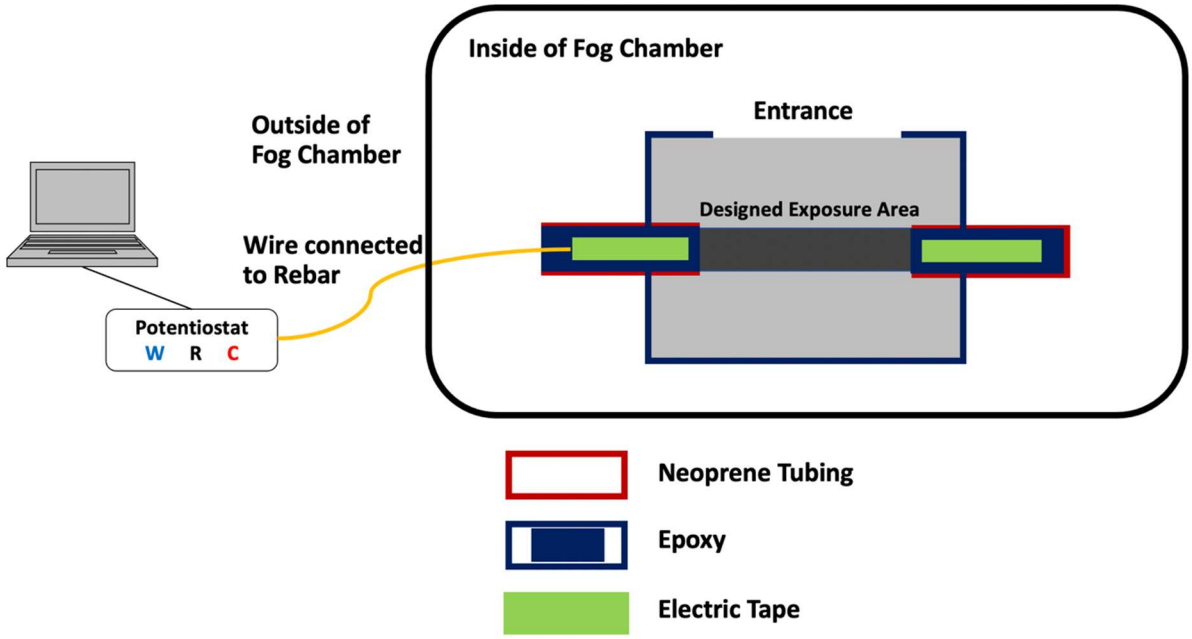

Figure 4. The Fog Chamber Test Setup

4.5. Materials Characterization

To gain a further understanding of the corrosion inhibiting mechanism of GPC, several techniques such as optical microscopy (OM), scanning electron microscopy (SEM), energy-dispersive X-ray spectroscopy (EDS), and X-ray diffraction (XRD) were used to analyze the micro-morphology and microstructure of the reinforced GPC concrete. OM is performed using DSX500 opto-digital microscope (Olympus, PA), and the images were taken and analyzed using the software from the same company. SEM and EDS were performed using the JEOL JSM-7500F (JEOL USA Inc, MA) FE-SEM, and the SEM images were taken with the JEOL SEM software while EDS were taken and analyzed using the INCA software. XRD is performed with the Bruker D8 X-ray (Bruker AXS LLC, WI) using Cu-Kα radiation.

5. ANALYSIS AND FINDINGS

5.1. Selection of Cement to Aggregate Ratio

The photographs of different GPC mixtures, labeled as #1-#4 in Table 3. It is important to note that the goal of this study is not to optimize OPC but rather using it as a quick and cost-efficient way to study the effect of cement to aggregate ratio. The details for each of the mix designs are listed in Table 2. As expected, use of more aggregate in the mixture, results in more porous the sample. This can be particular observed on the cross sections of Mix #1 and Mix#2 showing that the porosity does not just only appear on the surface but extends to the rest of the sample. After the visual inspections, Mix #1 was chosen as the optimal cement to aggregate ratio for making GPC concrete specimens for corrosion testing.

Table 3. Visuals of Different OPC Mix Designs.

Mix #1

Mix #2

Mix #3

Mix #4

Mix #1 – Cross Section

Mix #2 – Cross Section

To continue with the work, small specimens of GPC concrete with cement to aggregate ratio of Mix #1 were made. However, we ran into the issue of segregation when the specimens are vibrated, therefore, we opted to vacuum the specimens to minimize the porosity without segregation. The results from the two different methods are shown below in Figure 5.

Figure 5. Different Ways to Minimize Porosity in GPC Concrete.

5.2. Open Circuit Potential

The Figure 6 depicts the open circuit potential (OCP) trends over the testing period. Such indicates that if the embedded rebar is experiencing a corrosion regime or not. The potential difference between the standard reference electrode and the steel rebar as working electrode was correlated to assess the corrosion of the sample. In this experiment, the criterion suggested previously was applied to understand the regime that the rebar experiences as shown in Figure 7 (*56*).

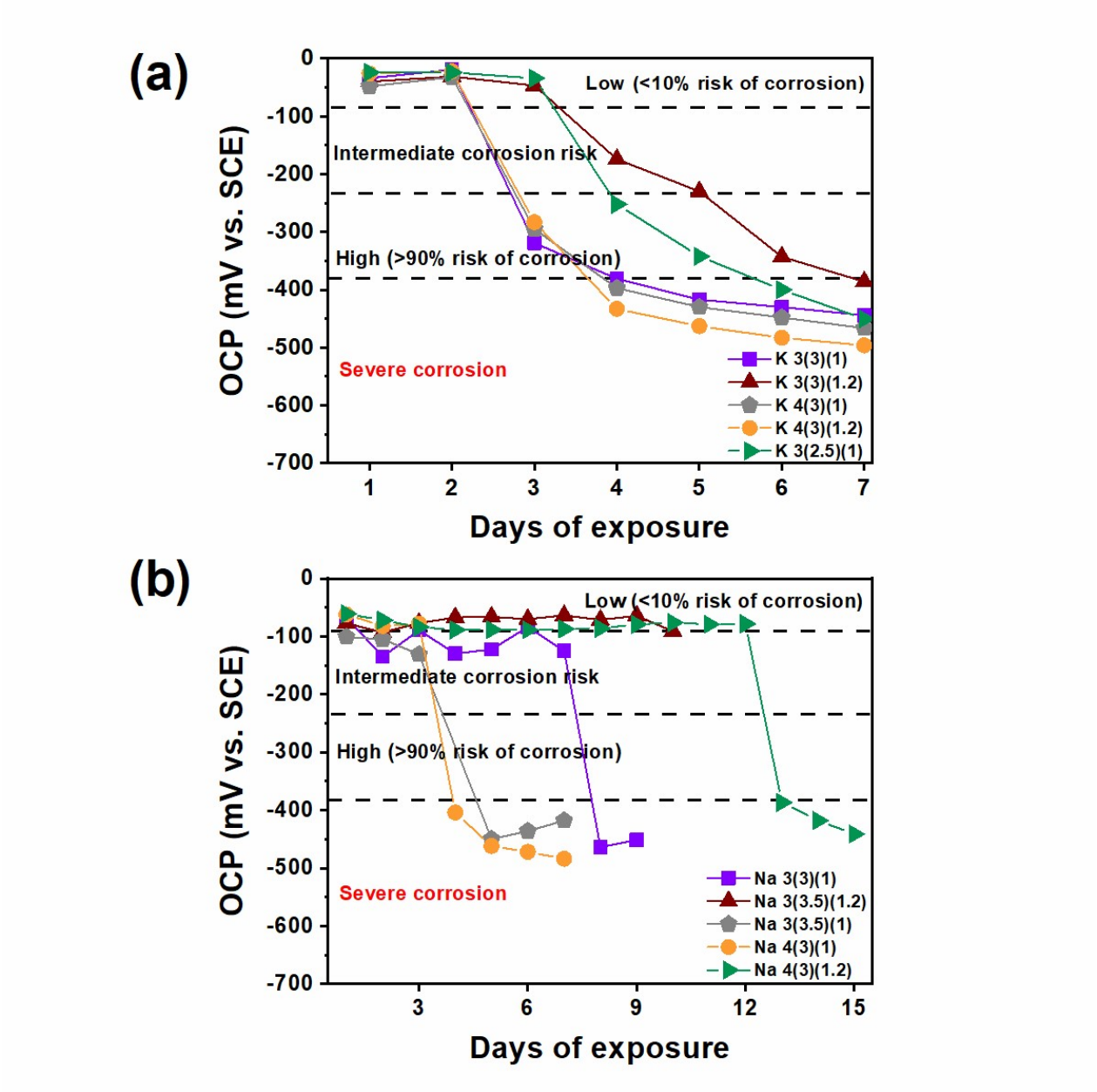

Figure 6. OCP of the (a) K-based GPCs and (b) Na-based GPCs during immersion test.

According to Figure 6, it is clear that Na-based GPCs have relatively better corrosion inhibiting performance compared to K-based GPCs, since it takes longer time for Na-based GPCs to reach the OCP value needed for severe corrosion. More specifically, the OCP of the K-based GPCs tended to decrease starting from 2nd or 3rd day of the immersion, while the Na-based GPC, especially the Na 4(3)(1.2) or Na 3(3.5)(1.2) showed considerably longer time before severe decrease in OCP, which can be considered as the 12th day of the immersion.

Copper/copper sulphate	*Silver/silver chloride/ 1.0M KCl*	*Standard hydrogen electrode*	*Calomel*	*Corrosion condition*
>−200 mV	>−100 mV	+120 mV	>−80 mV	Low (10% risk of corrosion)
−200 to −350 mV	−100 to −250 mV	+120 to −30 mV	−80 mV to −230 mV	Intermediate corrosion risk
<−350 mV	<−250 mV	−30 mV	<−230 mV	High (>90% risk of corrosion)
<−500 mV	<−400 mV	−180 mV	<−380 mV	Severe corrosion

Figure 7. ASTM corrosion criteria for reinforced concrete.

It is also observable that the OCP of the K-based samples shows more gradual decrease when compared to that of the Na-based samples which showed abrupt decrease of the OCP values. Such this feature possibly derived from the precipitation of the KCl on the surface of the GPC samples which will be further discussed in the later section (5.5.1. X-ray Diffraction). In another words, the exchange of K cations between in GP matrix of GPC whit Na from electrolyte most likely take place, during electrolyte diffusion, and the K precipitated KCl on the surface of the sample. Precipitation of KCl decreased the chlorine concentration nearby the rebar so the passive layer can be degraded gradually before cation reacting was completed, but the continued supply of the high-concentration of NaCl solution finally introduced the severe corrosion regime of the rebar regardless of the composition of the K-based GPCs. In the Na-based GPCs, such gradual decrease of the OCP is not observable. Instead, rather abrupt decrease of OCP value from low to intermediate to severe corrosion level in a day. This can be explained by a lack of consumption of chloride ions due to cation exchange. Thus, once the concrete matrix barrier is penetrated by the supplied electrolyte, the rebar reacts with the electrolyte with high chloride concentration that leads to enter the severe corrosion regime directly.

5.3. Electrochemical Impedance Spectroscopy

Figure 9 to Figure 18 represents the Nyquist and Bode plots of the tested samples obtained by EIS testing. Regardless of the base cation, the early-period Nyquist plots have the same shape as the typical impedance plots for concrete samples. This general shape of the plot illustrated in Figure 8 suggests the existence of three elements, namely concrete bulk, bulk-electrode hybrid, and electrode interface (*57*). Up until the concrete matrix allows the water penetration fully toward the rebar, the tail part of the Nyquist was observed. It is also noticeable that the real value of the impedance, shown as $Z^{'}$, decreases dramatically after the immersion started, and this is due to the electrolyte uptake through the concrete matrix. Hence, as the electrolyte penetrates more of the concrete matrix, the real part of the impedance decreases as a result. Such decrease of the real part of the impedance value converges in a certain value range, around 3-5 kohm-cm^2, and as the concrete allows more of the electrolyte penetration, it is also observable that the system of the concrete bulk diminishes by the abundance of electrolyte that it contains. As a result, the water residing inside of the concrete matrix reaches the rebar to initiate the rebar degradation known as corrosion, represented by decreasing size and angle of the tail part of the impedance plot.

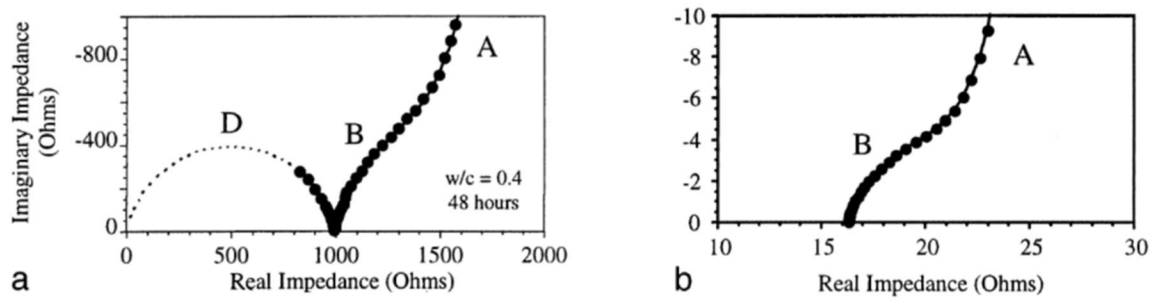

Figure 8. Nyquist plots of carbon steel electrodes in (a) Ordinary Portland Cement and (b) Synthetic Pore Solution.

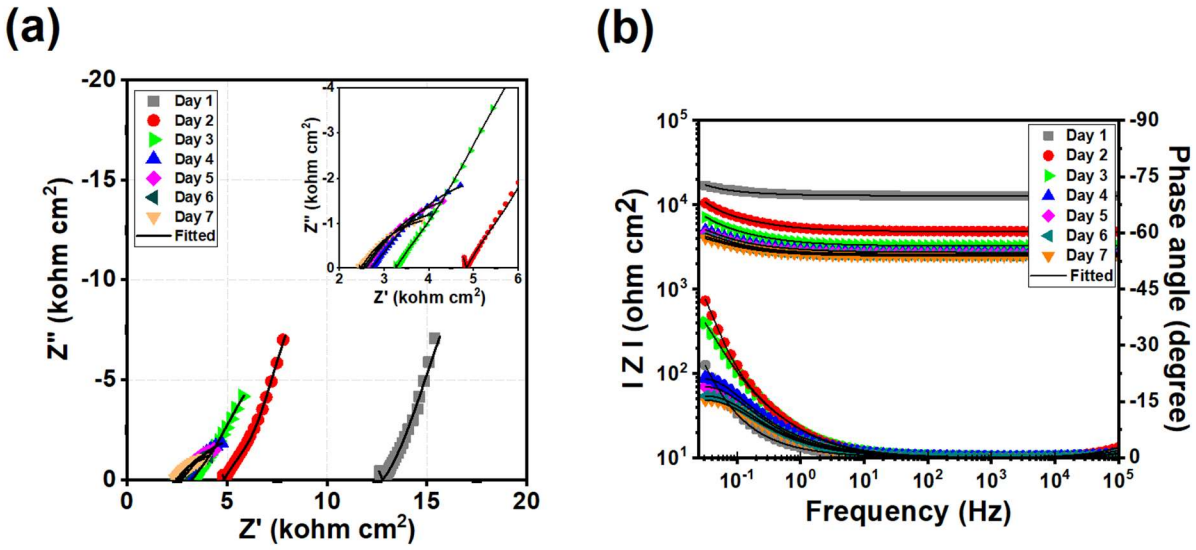

Figure 9. (a) Nyquist Plot and (b) Bode Plot of sample K43(1.2).

The Nyquist plots are in good agreement previously shown OCP plots. More specifically, there is no noticeable change of the tail part of the impedance plot when the water penetration did not reach to the rebar itself. Thus, the OCP value still maintains at the passive level of low-risk corrosion regime. However, when water uptakes through the concrete matrix and finally reaches to the rebar, the electrochemical reactions initiate and the breakage of the passivation layer of the rebar occurs, resulting in the decrease of the OCP gradually. This feature is also reflected in the Nyquist plot at the longer period of immersion as the depressed tail part. Such depressed part also showed considerably decreased impedance modulus, representable of the decreased corrosion resistance of the system.

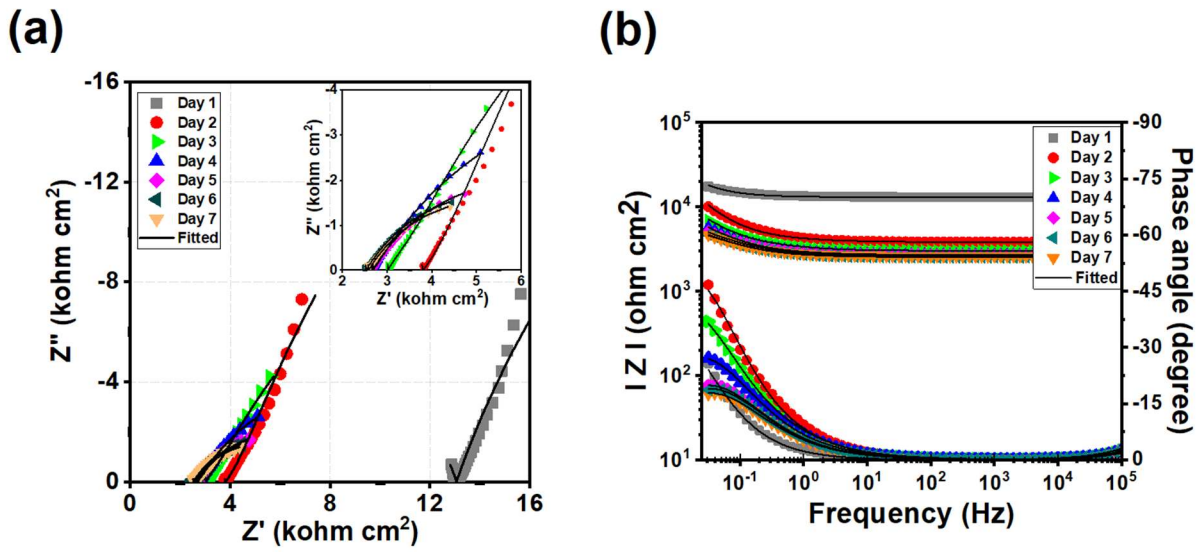

Figure 10. (a) Nyquist Plot and (b) Bode Plot of sample K331.

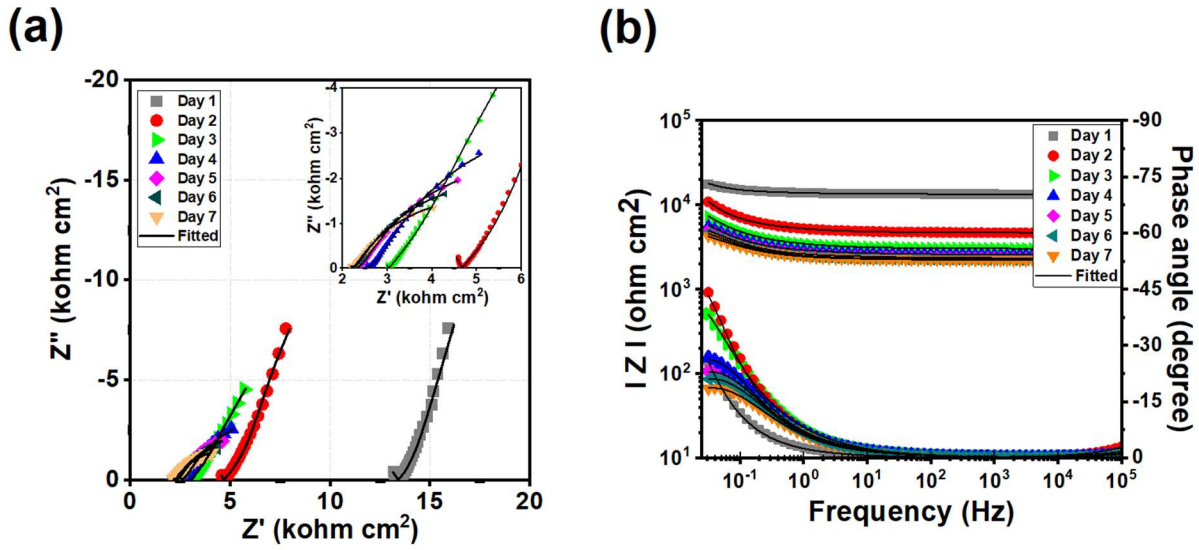

Figure 11. (a) Nyquist Plot and (b) Bode Plot of sample K431.

As previously mentioned, the different degradation trends of the K- or Na- based GPC samples are also observable in the Nyquist plots. In case of the K-based GPCs, the decrease of the tail part of the impedance plot is gradual as the size of the tail part decreases gradually over time. Meanwhile, in the Na-based GPCs, the decrease of tail part is more abrupt, which is due to of the Cl- concentrated electrolyte uptake to the rebar surface.

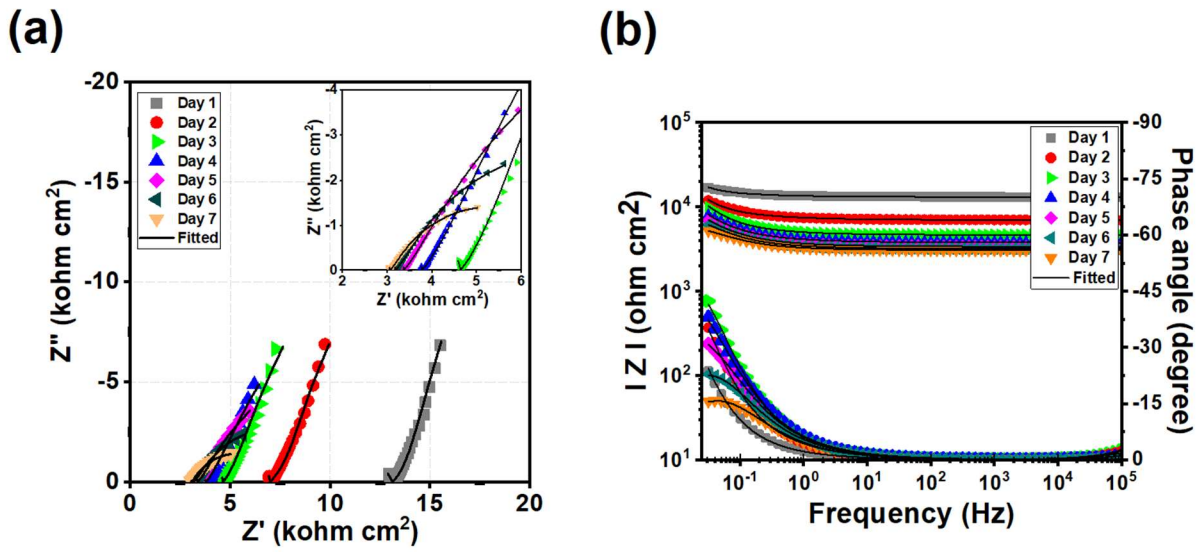

Figure 12. (a) Nyquist Plot and (b) Bode Plot of sample K3(2.5)1.

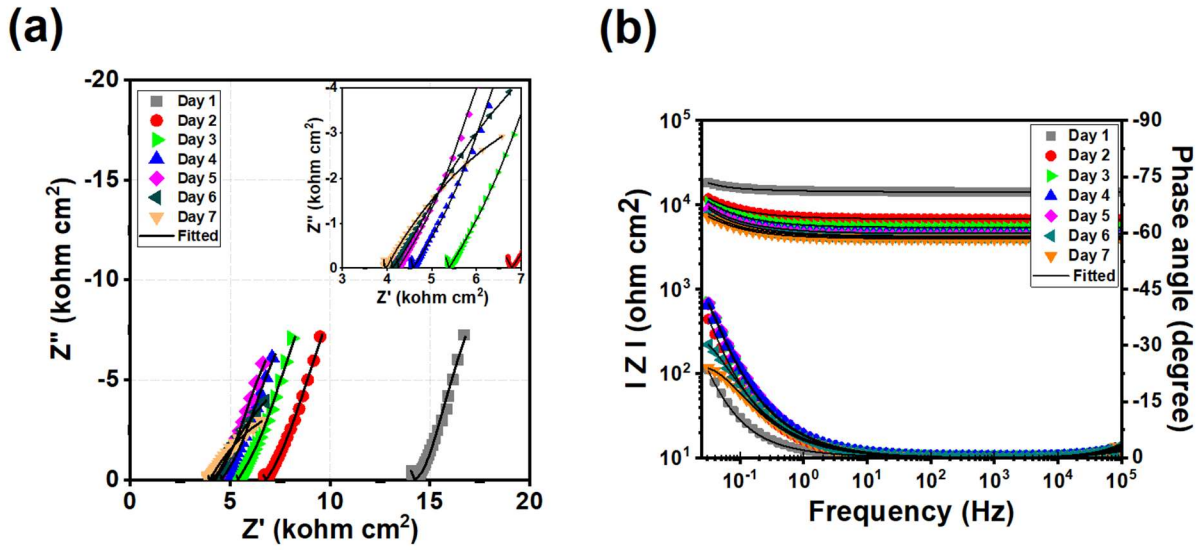

Figure 13. (a) Nyquist Plot and (b) Bode Plot of sample K33(1.2).

The Bode plots of the samples also indicates a similar trend, but with more detailed information of the surface condition. In general, compared to the K-based GPCs that shows the rise of phase angle up to 45 degree then decrease towards the lower values, the Na-based GPCs showed higher peak phase angle up to 60 degree which possibly indicate that the rebar is more electrochemically stable with maintaining well-ordered passive layer thus contributing to the better corrosion resistance. However, even in the Na-based GPCs, the phase angles tended to decrease towards the lower value which is indicative of the more active charge transfer reactions. The decrease of the phase angle which represents more active electrochemical reactions is attributed to the chloride ions that helps the dissolution of the rebar substrate. As previously mentioned, the filtration of the

chloride ion by the K-based GPC matrix may have helped with the relieving the concentration of such ion which possibly resulted in the slower decrease of the phase angle at the lower frequency region. Hence, the chloride concentration may not heavily exceed the critical chloride concentration of the rebar and thus, the corrosion precede more in a slower manner. Meanwhile in the Na-based GPCs, there was no filtration of Cl in the GPC matrix, possibly allowing the high concentration of electrolyte itself without any pre-treatment of chloride filtration. Thus, the rebar might have exposed to the electrolyte with high chloride concentration that possibly occurred an abrupt decrease of the corrosion resistance represented as an abrupt decrease of the phase angle at low frequency range.

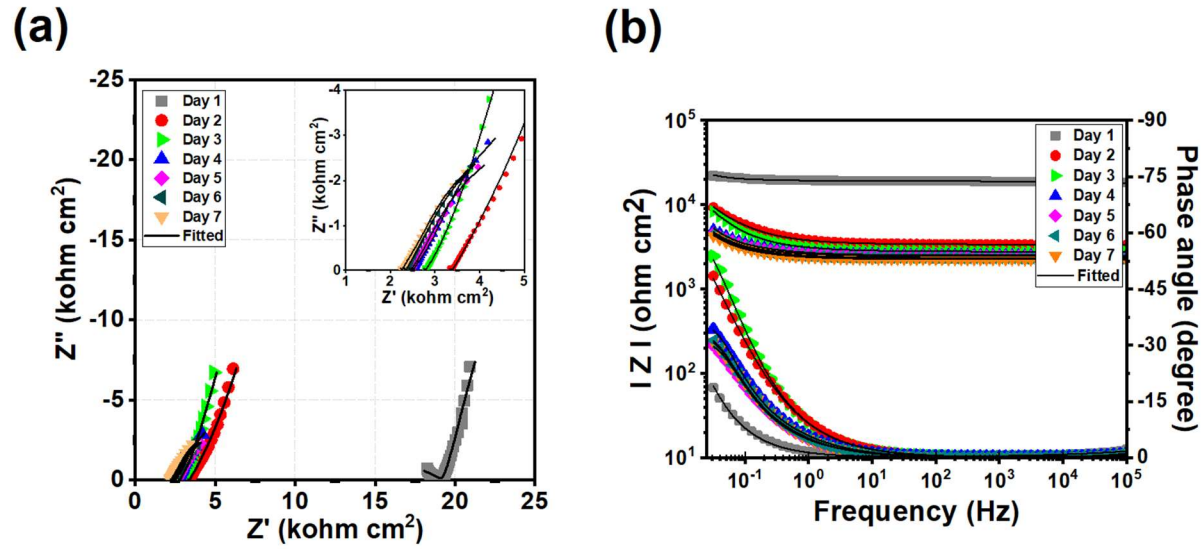

Figure 14. (a) Nyquist Plot and (b) Bode Plot of sample Na431.

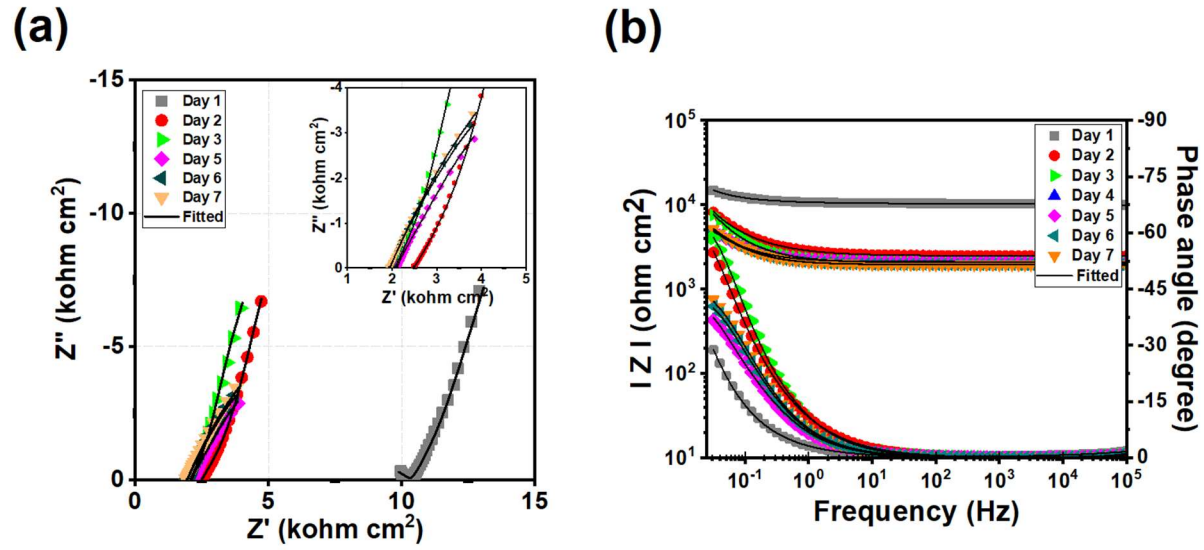

Figure 15. (a) Nyquist Plot and (b) Bode Plot of sample Na3(3.5)1.

Among the K-based GPCs, the K33(1.2) and K3(2.5)1 showed the best anti-corrosion performance in the phase 1 test with 14 days of curing with 7 days of each wet and dry curing, respectively. Such samples also showed the delayed rebar degradation shown in the Nyquist and Bode plots compared to the other K-based GPC samples. Such results may reveal the better filtering capability and barrier protection in such composition based of the K higher concentration of K cations in tose GPs. Compared to the K331, the K33(1.2) and K3(2.5)1 have more of cation and less of porosity, respectively, and such result may have affected from the change of such parameters. More of cation may worked to form more compact concrete matrix, and the less of water used in preparing GP binder results in less porous matrix.

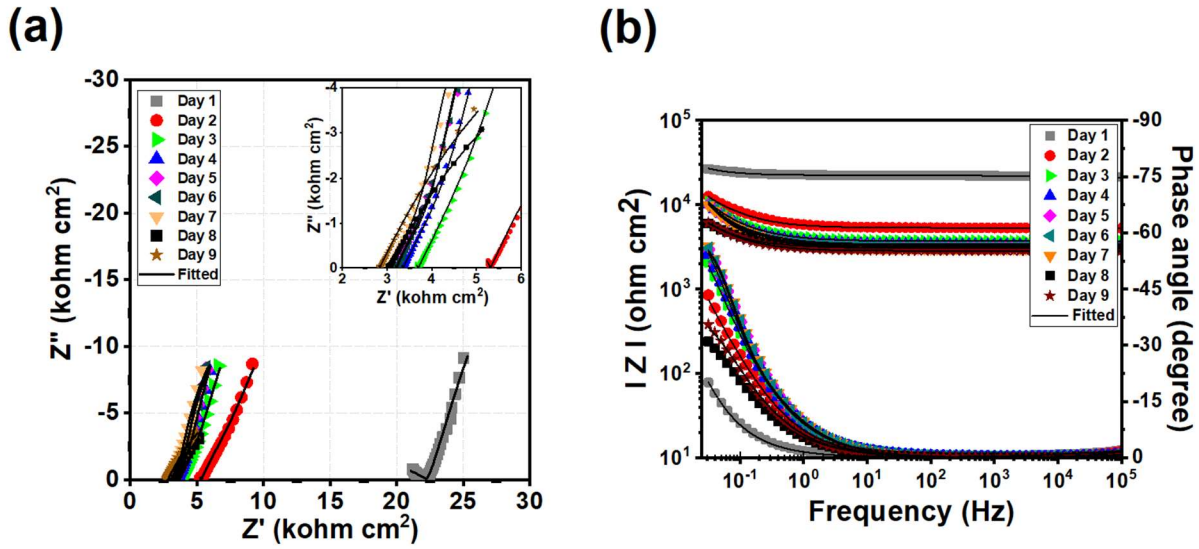

Figure 16. (a) Nyquist Plot and (b) Bode Plot of sample Na331.

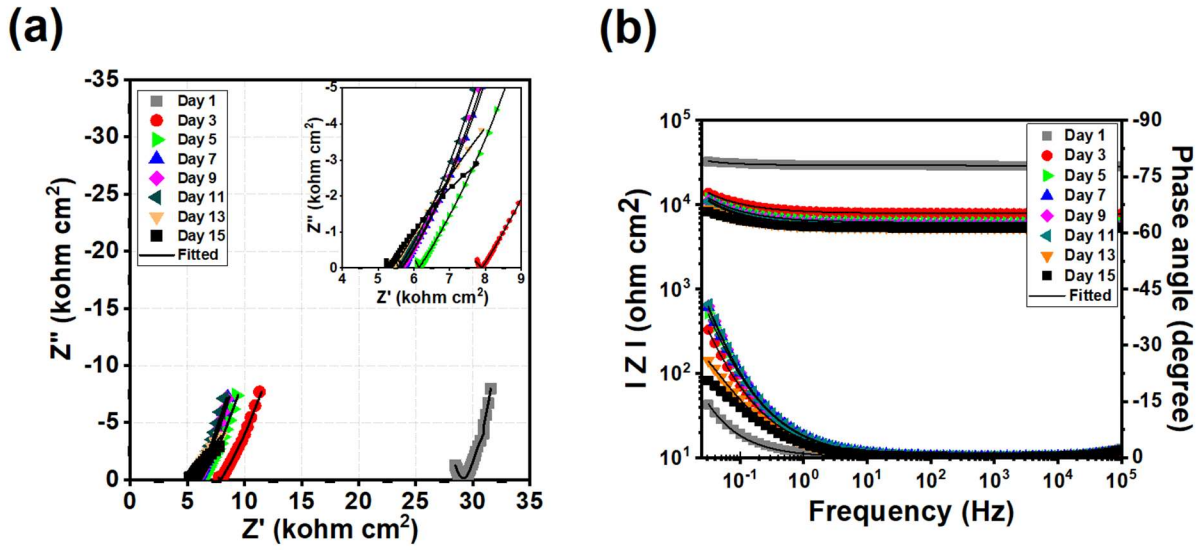

Figure 17. (a) Nyquist Plot and (b) Bode Plot of sample Na43(1.2).

In the case of Na-based GPCs, the Na3(3.5)(1.2) and Na43(1.2) showed the best anti-corrosion performance in the phase-1 test with 14 days of curing with 7 days of each wet and dry curing, respectively. Those samples also showed the delayed rebar degradation even when compared to the K-base GPCs in all the electrochemical-based tests. The Na3(3.5)(1.2) higher Na concentration when compared to Na3(3.5)1 which had entered the corrosion regime earlier. It can be estimated that the extra cation supplied may have helped with forming a denser concrete matrix that contributed to enhance barrier protection of such concrete matrix and that access Na helped with Cl uptake. In case of Na43(1.2) sample, it had more of sodium cation when compared to Na431 that entered the corrosion regime before day 4.

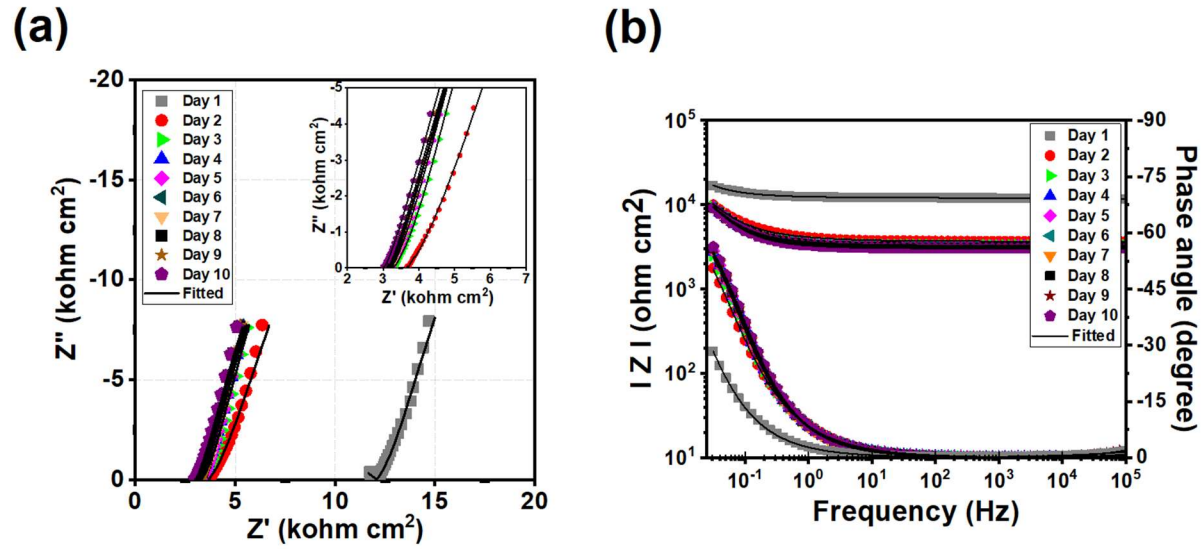

Figure 18. (a) Nyquist Plot and (b) Bode Plot of sample Na3(3.5)(1.2).

5.4. Deterministic Modeling

Following the electrochemical results, we were able to propose a mechanism base on the dynamics of the interface. The interfacial reactions of the electrolyte up-taking the geopolymer matrix are characterized by EIS. Due to the number of experiments and parameters involved the variability is not considered for this effort. The probabilistic approach is not performed due to the nature of the mechanism. Deterministic approach was implemented based on the elements of the electrochemical system (aqueous electrolyte, solid electrolyte-geopolymer- and rebar) could be studied by deterministic modeling. The theoretical modeling with RC elements and electrolyte characteristics, as well as their validation with electrochemical and concrete testing, allows quantitative approach in regards of the concrete degradation. A simple model based on rebar/concrete interface analysis and real-time monitoring characterization in corrosive environment helped to develop a deterministic approach, as illustrated in this section. Due to the relatively fast material degradation of the GPC compared to that of conventional OPC, the merit that comes from the probabilistic modeling is not considerable as much as the one from the

deterministic modeling, therefore only the deterministic modeling has been studied to better understand the concrete degradation in a quantitative manner.

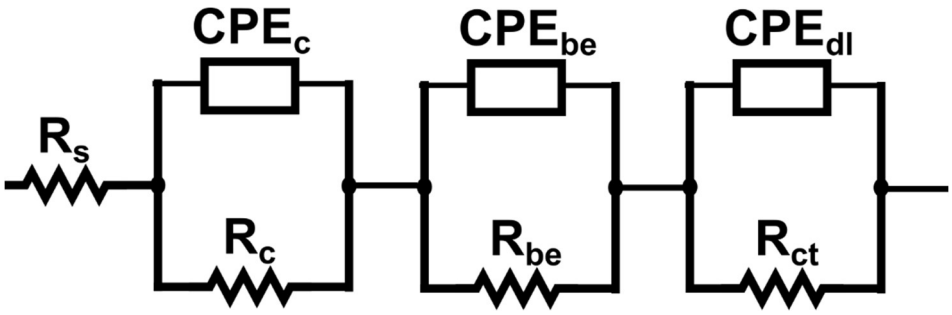

Figure 19. Equivalent circuit for GPC system.

An equivalent circuit (EC) model is suggested as shown in Figure 19 to provide effective parameters quantitatively in the corroding system. The impedance spectra that included the concrete bulk, bulk-electrode hybrid, and electrode interface are allocated for each segment of the equivalent circuit component, respectively. The ECs included elements, namely, the solution resistance (R_s), concrete bulk resistance (R_c), bulk-electrode resistance (R_{be}), charge-transfer resistance (R_{ct}), capacitance in terms of the constant phase element (CPE), concrete bulk pore capacitance (C_c), bulk-electrode capacitance (C_{be}), and double-layer capacitance (C_{dl}). The CPE concept was introduced to represent the depressed impedance semicircles, which is known to be occurred from the various physical properties of the concrete resulting in the time constants distributions (*58; 59; 61*). The CPE capacitance can be described as below

$$C = Y_0(\omega''_{max})^{n-1} \quad [1]$$

where Y_0 and $0 < n \leq 1$ are the model parameters, and ω''_{max} is the angular frequency at the maximum imaginary impedance Z''.

The quantified impedance parameters obtained from the aforementioned ECs are summarized in Table 4. At the initial immersion period, the Na-based GPCs showed relatively higher polarization resistance, $R_p = R_c + R_{be} + R_{ct}$, which represents a better barrier performance in such period. The K-based GPC samples revealed at around 100 kohm-cm^2 initial polarization resistance, while the Na-based GPC samples showed higher values up to 140 kohm-cm^2 range. Over the prolonged immersion period, the polarization resistance tended to decrease as the water started to penetrate the concrete matrix which is represented as the decrease of concrete bulk resistance and bulk-electrode resistance. The charge-transfer resistance that represents the resistance of the target of interest, such as rebar surface, has been maintained relatively more intact compare to the concrete matrix resistance parameters. Nevertheless, as the water penetrates deeper part of the concrete, the charge-transfer resistance also tended to be decreased over time.

Table 4. Impedance parameters for the GPC samples immersed in 3.5 wt.% NaCl electrolyte.

Time (day)	R_c ($\Omega\ cm^2$)	C_c ($F\ cm^{-2}\ s^{n-1}$)	n_c	R_{be} ($\Omega\ cm^2$)	C_{be} ($F\ cm^{-2}\ s^{n-1}$)	n_{be}	R_{ct} ($\Omega\ cm^2$)	C_{dl} ($F\ cm^{-2}\ s^{n-1}$)	n_{dl}	R_p ($\Omega\ cm^2$)
K331										
1	1.45×10^4	6.75×10^{-4}	0.533	1.30×10^4	4.70×10^{-11}	0.855	7.20×10^4	8.56×10^{-4}	1	9.95×10^4

2	2.09×10^{3}	8.97×10^{-4}	0.500	3.79×10^{3}	4.79×10^{-11}	0.905	6.35×10^{4}	5.22×10^{-4}	0.860	6.93×10^{4}
3	3.98×10^{2}	1.09×10^{-3}	0.650	3.01×10^{3}	2.21×10^{-11}	1	3.97×10^{4}	6.55×10^{-4}	0.744	4.31×10^{4}
4	7.69×10^{1}	2.74×10^{-3}	0.677	2.68×10^{3}	2.60×10^{-11}	1	1.23×10^{4}	7.40×10^{-4}	0.695	4.31×10^{4}
5	6.63×10^{0}	4.95×10^{-3}	0.534	2.66×10^{3}	5.71×10^{-11}	0.932	6.68×10^{3}	8.34×10^{-4}	0.669	9.35×10^{3}
6	1.17×10^{0}	4.05×10^{-3}	0.480	2.52×10^{3}	5.90×10^{-11}	0.941	5.84×10^{3}	8.90×10^{-4}	0.666	8.37×10^{3}
7	1.57×10^{0}	4.03×10^{-3}	0.471	2.57×10^{3}	5.75×10^{-11}	0.942	5.33×10^{3}	9.31×10^{-4}	0.665	7.91×10^{3}
K33(1.2)										
1	1.60×10^{4}	9.37×10^{-4}	0.389	1.42×10^{4}	7.54×10^{-11}	0.775	6.89×10^{4}	7.39×10^{-4}	0.957	9.91×10^{4}
2	6.05×10^{3}	6.16×10^{-4}	0.567	6.77×10^{3}	2.71×10^{-10}	0.745	6.74×10^{4}	8.46×10^{-4}	1	8.03×10^{4}
3	3.98×10^{3}	5.62×10^{-4}	0.604	5.37×10^{3}	8.49×10^{-11}	0.860	5.73×10^{4}	8.07×10^{-4}	1	6.66×10^{4}
4	2.61×10^{3}	6.04×10^{-4}	0.611	4.56×10^{3}	5.35×10^{-11}	0.912	3.47×10^{4}	8.63×10^{-4}	1	4.19×10^{4}
5	2.37×10^{3}	6.43×10^{-4}	0.619	4.24×10^{3}	4.65×10^{-11}	0.933	3.32×10^{4}	9.06×10^{-4}	1	3.98×10^{4}
6	1.97×10^{3}	9.88×10^{-4}	0.534	4.10×10^{3}	5.08×10^{-11}	0.941	1.45×10^{4}	1.02×10^{-3}	0.901	2.06×10^{4}
7	1.20×10^{3}	1.38×10^{-3}	0.494	3.94×10^{3}	4.68×10^{-11}	0.957	8.58×10^{3}	9.73×10^{-4}	0.843	1.37×10^{4}
K3(2.5)1										
1	1.49×10^{4}	7.76×10^{-4}	0.465	1.31×10^{4}	2.11×10^{-10}	0.707	6.22×10^{4}	8.86×10^{-4}	1	9.02×10^{4}
2	2.99×10^{3}	6.26×10^{-4}	0.517	6.99×10^{3}	7.15×10^{-11}	0.850	4.22×10^{4}	7.37×10^{-4}	0.970	5.22×10^{4}
3	2.77×10^{3}	8.18×10^{-4}	0.523	4.63×10^{3}	8.66×10^{-11}	0.874	4.21×10^{4}	6.93×10^{-4}	0.934	4.96×10^{4}
4	2.22×10^{3}	1.09×10^{-3}	0.484	3.76×10^{3}	2.89×10^{-11}	0.910	3.88×10^{4}	8.11×10^{-4}	0.853	4.48×10^{4}
5	2.28×10^{3}	1.73×10^{-3}	0.424	3.36×10^{3}	9.38×10^{-11}	1	1.69×10^{4}	8.79×10^{-4}	0.794	2.25×10^{4}
6	5.39×10^{2}	1.83×10^{-3}	0.449	3.17×10^{3}	1.03×10^{-10}	1	7.36×10^{3}	8.94×10^{-4}	0.782	1.10×10^{4}
7	2.63×10^{2}	3.98×10^{-3}	0.344	3.05×10^{3}	1.09×10^{-10}	1	4.21×10^{3}	9.62×10^{-4}	0.736	7.52×10^{3}
K43(1.2)										
1	1.44×10^{4}	6.24×10^{-4}	0.541	1.27×10^{4}	9.84×10^{-11}	0.768	7.34×10^{4}	9.76×10^{-4}	1	1.00×10^{5}
2	2.76×10^{3}	3.89×10^{-4}	0.666	4.83×10^{3}	1.20×10^{-10}	0.851	5.04×10^{4}	7.47×10^{-4}	1	5.80×10^{4}
3	1.53×10^{3}	7.06×10^{-4}	0.615	3.25×10^{3}	1.86×10^{-11}	0.961	3.34×10^{4}	9.29×10^{-4}	0.858	3.82×10^{4}
4	3.27×10^{2}	1.31×10^{-3}	0.605	2.71×10^{3}	1.25×10^{-11}	0.991	5.96×10^{3}	1.07×10^{-3}	0.767	9.01×10^{3}
5	2.01×10^{2}	2.57×10^{-3}	0.490	2.56×10^{3}	3.94×10^{-11}	0.912	4.92×10^{3}	1.14×10^{-3}	0.737	7.68×10^{3}
6	1.08×10^{2}	2.66×10^{-3}	0.492	2.50×10^{3}	1.47×10^{-10}	0.817	4.04×10^{3}	1.25×10^{-3}	0.711	6.65×10^{3}
7	5.72×10^{1}	3.78×10^{-3}	0.457	2.45×10^{3}	8.96×10^{-11}	0.859	3.70×10^{3}	1.26×10^{-3}	0.690	6.21×10^{3}
K431										
1	1.56×10^{4}	6.54×10^{-4}	0.485	1.34×10^{4}	5.51×10^{-10}	0.634	7.55×10^{4}	8.25×10^{-4}	1	1.05×10^{5}
2	3.88×10^{3}	4.95×10^{-4}	0.522	4.66×10^{3}	6.56×10^{-10}	0.734	4.08×10^{4}	7.32×10^{-4}	1	4.94×10^{4}
3	1.70×10^{3}	7.47×10^{-4}	0.526	3.03×10^{3}	2.01×10^{-9}	0.619	3.51×10^{4}	8.40×10^{-4}	0.850	3.98×10^{4}
4	3.15×10^{2}	8.22×10^{-4}	0.515	2.57×10^{3}	1.38×10^{-9}	0.653	9.08×10^{3}	8.10×10^{-4}	0.759	1.19×10^{3}
5	1.58×10^{2}	9.62×10^{-4}	0.497	2.33×10^{3}	9.27×10^{-10}	0.688	6.98×10^{3}	8.40×10^{-4}	0.715	9.47×10^{3}
6	9.81×10^{1}	1.08×10^{-3}	0.479	2.23×10^{3}	8.34×10^{-10}	0.702	6.06×10^{3}	8.75×10^{-4}	0.688	8.38×10^{3}
7	6.78×10^{1}	1.02×10^{-3}	0.483	2.19×10^{3}	6.61×10^{-10}	0.728	5.08×10^{3}	9.42×10^{-4}	0.665	7.35×10^{3}
Na331										
1	3.65×10^{4}	6.25×10^{-4}	0.657	2.23×10^{4}	3.29×10^{-10}	0.337	7.54×10^{4}	8.60×10^{-4}	1	1.34×10^{5}
2	6.17×10^{3}	4.34×10^{-4}	0.679	5.29×10^{3}	3.12×10^{-10}	0.738	7.22×10^{4}	7.63×10^{-4}	1	8.37×10^{4}
3	3.41×10^{3}	5.36×10^{-4}	0.656	3.68×10^{3}	3.33×10^{-10}	0.711	6.78×10^{4}	6.64×10^{-4}	1	7.49×10^{4}
4	2.17×10^{3}	5.49×10^{-4}	0.662	3.34×10^{3}	8.69×10^{-11}	0.820	6.49×10^{4}	6.23×10^{-4}	1	7.05×10^{4}
5	1.37×10^{3}	5.16×10^{-4}	0.732	3.18×10^{3}	6.26×10^{-11}	0.849	4.76×10^{4}	5.81×10^{-4}	1	5.21×10^{4}
6	1.17×10^{3}	4.99×10^{-4}	0.745	3.21×10^{3}	9.41×10^{-10}	0.644	4.36×10^{4}	5.78×10^{-4}	1	4.80×10^{4}
7	1.09×10^{3}	5.37×10^{-4}	0.727	3.04×10^{3}	9.44×10^{-10}	0.650	4.08×10^{4}	5.88×10^{-4}	1	4.50×10^{4}
8	1.94×10^{2}	2.06×10^{-3}	0.658	3.03×10^{3}	3.99×10^{-10}	0.708	1.60×10^{4}	8.70×10^{-4}	0.777	1.93×10^{4}
9	3.24×10^{2}	2.66×10^{-3}	0.689	2.82×10^{3}	7.63×10^{-11}	0.842	1.99×10^{4}	8.45×10^{-4}	0.794	2.30×10^{4}

Na3(3.5)1										
1	5.17×10^{3}	6.06×10^{-4}	0.579	1.03×10^{4}	3.84×10^{-10}	0.369	7.67×10^{4}	8.39×10^{-4}	1	9.22×10^{4}
2	2.68×10^{3}	6.24×10^{-4}	0.613	2.47×10^{3}	1.20×10^{-11}	1	7.34×10^{4}	8.13×10^{-4}	1	7.88×10^{4}
3	1.37×10^{3}	8.04×10^{-4}	0.680	2.05×10^{3}	1.19×10^{-11}	1	4.69×10^{4}	7.79×10^{-4}	1	5.04×10^{4}
5	1.45×10^{3}	1.18×10^{-3}	0.714	2.09×10^{3}	1.42×10^{-10}	0.637	9.72×10^{3}	1.85×10^{-3}	1	1.33×10^{4}
6	1.95×10^{3}	1.26×10^{-3}	0.705	1.94×10^{3}	5.49×10^{-10}	0.721	1.03×10^{4}	1.81×10^{-3}	1	1.42×10^{4}
7	2.68×10^{3}	1.18×10^{-3}	0.686	1.93×10^{3}	6.57×10^{-9}	0.537	1.18×10^{4}	1.80×10^{-3}	1	1.64×10^{4}
Na431										
1	2.56×10^{4}	9.59×10^{-4}	0.610	1.92×10^{4}	5.55×10^{-10}	0.312	7.56×10^{4}	9.37×10^{-4}	1	1.20×10^{5}
2	5.48×10^{3}	5.56×10^{-4}	0.617	3.38×10^{3}	1.72×10^{-7}	0.279	7.42×10^{4}	9.05×10^{-4}	1	8.31×10^{4}
3	5.08×10^{3}	7.58×10^{-4}	0.572	2.77×10^{3}	2.91×10^{-9}	0.576	7.28×10^{4}	9.02×10^{-4}	1	8.21×10^{4}
4	9.70×10^{2}	1.05×10^{-3}	0.640	2.50×10^{3}	6.34×10^{-11}	0.879	8.07×10^{3}	1.59×10^{-3}	1	1.15×10^{4}
5	1.23×10^{3}	1.50×10^{-3}	0.584	2.44×10^{3}	4.99×10^{-10}	0.729	5.52×10^{3}	2.05×10^{-3}	1	9.19×10^{3}
6	1.07×10^{3}	1.48×10^{-3}	0.621	2.33×10^{3}	4.44×10^{-10}	0.742	6.06×10^{3}	2.07×10^{-3}	1	9.46×10^{3}
7	8.45×10^{2}	1.39×10^{-3}	0.671	2.25×10^{3}	7.76×10^{-10}	0.707	5.89×10^{3}	2.11×10^{-3}	1	8.99×10^{3}
Na43(1.2)										
1	3.45×10^{4}	7.33×10^{-4}	0.540	2.92×10^{4}	1.43×10^{-9}	0.534	7.67×10^{4}	8.36×10^{-4}	1	1.40×10^{5}
3	6.91×10^{3}	4.54×10^{-4}	0.615	7.90×10^{3}	4.85×10^{-9}	0.510	7.64×10^{4}	8.46×10^{-4}	1	9.12×10^{4}
5	6.45×10^{3}	4.91×10^{-4}	0.598	6.13×10^{3}	3.22×10^{-10}	0.734	7.64×10^{4}	8.63×10^{-4}	1	8.90×10^{4}
7	5.95×10^{3}	5.37×10^{-4}	0.584	5.66×10^{3}	1.12×10^{-10}	0.819	7.64×10^{4}	8.63×10^{-4}	1	8.80×10^{4}
9	5.81×10^{3}	5.55×10^{-4}	0.584	5.64×10^{3}	1.42×10^{-10}	0.803	7.63×10^{4}	8.72×10^{-4}	1	8.78×10^{4}
11	6.00×10^{3}	5.81×10^{-4}	0.576	5.55×10^{3}	1.21×10^{-10}	0.829	7.63×10^{4}	8.72×10^{-4}	1	8.79×10^{4}
13	1.67×10^{3}	1.46×10^{-3}	0.461	5.34×10^{3}	5.91×10^{-11}	0.878	2.66×10^{4}	8.49×10^{-4}	0.788	3.37×10^{4}
15	8.64×10^{2}	1.76×10^{-3}	0.429	5.23×10^{3}	1.11×10^{-10}	0.832	1.20×10^{4}	8.68×10^{-4}	0.766	1.82×10^{4}
Na3(3.5)(1.2)										
1	1.81×10^{4}	6.50×10^{-4}	0.544	1.21×10^{4}	1.05×10^{-8}	0.440	7.65×10^{4}	8.39×10^{-4}	1	1.40×10^{5}
2	1.66×10^{4}	6.39×10^{-4}	0.523	3.66×10^{3}	9.61×10^{-11}	0.780	7.64×10^{4}	8.53×10^{-4}	1	9.12×10^{4}
3	1.41×10^{4}	8.11×10^{-4}	0.536	3.27×10^{3}	2.15×10^{-10}	0.741	7.64×10^{4}	8.21×10^{-4}	1	8.90×10^{4}
4	1.38×10^{4}	8.55×10^{-4}	0.558	3.17×10^{3}	2.93×10^{-10}	0.710	7.61×10^{4}	8.35×10^{-4}	1	8.80×10^{4}
5	1.22×10^{4}	8.64×10^{-4}	0.578	3.21×10^{3}	3.50×10^{-10}	0.698	7.61×10^{4}	8.37×10^{-4}	1	8.78×10^{4}
6	1.12×10^{4}	8.44×10^{-4}	0.593	3.12×10^{3}	3.81×10^{-10}	0.705	7.61×10^{4}	8.44×10^{-4}	1	8.79×10^{4}
7	1.12×10^{4}	8.51×10^{-4}	0.619	3.19×10^{3}	3.63×10^{-10}	0.707	7.61×10^{4}	8.57×10^{-4}	1	3.37×10^{4}
8	1.08×10^{4}	8.60×10^{-4}	0.626	3.12×10^{3}	3.32×10^{-10}	0.731	7.61×10^{4}	8.64×10^{-4}	1	1.82×10^{4}
9	1.06×10^{4}	8.54×10^{-4}	0.623	3.16×10^{3}	3.53×10^{-10}	0.782	7.61×10^{4}	8.56×10^{-4}	1	1.82×10^{4}
10	9.68×10^{3}	8.70×10^{-4}	0.617	3.01×10^{3}	3.55×10^{-10}	0.710	7.61×10^{4}	8.49×10^{-4}	1	1.82×10^{4}

As discussed earlier, the decreasing trend of the polarization resistance shows some differences, depending on the type of activation cations in GPC matrix, as it is illustrated in Figure 20. In case of K-based samples, even though its initial polarization resistance was lower than that of the Na-based GPCs, it revealed gradual decrease of the polarization resistance over time. This might be attributed to the limited chloride ion supply due to cation exchanging action in K-based GPC matrix. Even though such K-based GPC allowed relatively faster water penetration through the concrete matrix and the loss of polarization resistance tends to appear gradually over the period of a few days period. This may be triggered by the limited supply of the chloride ion in the initial immersion period, followed by continued chloride ion supply with its accumulation that finally far exceeded the critical chloride ion concentration.

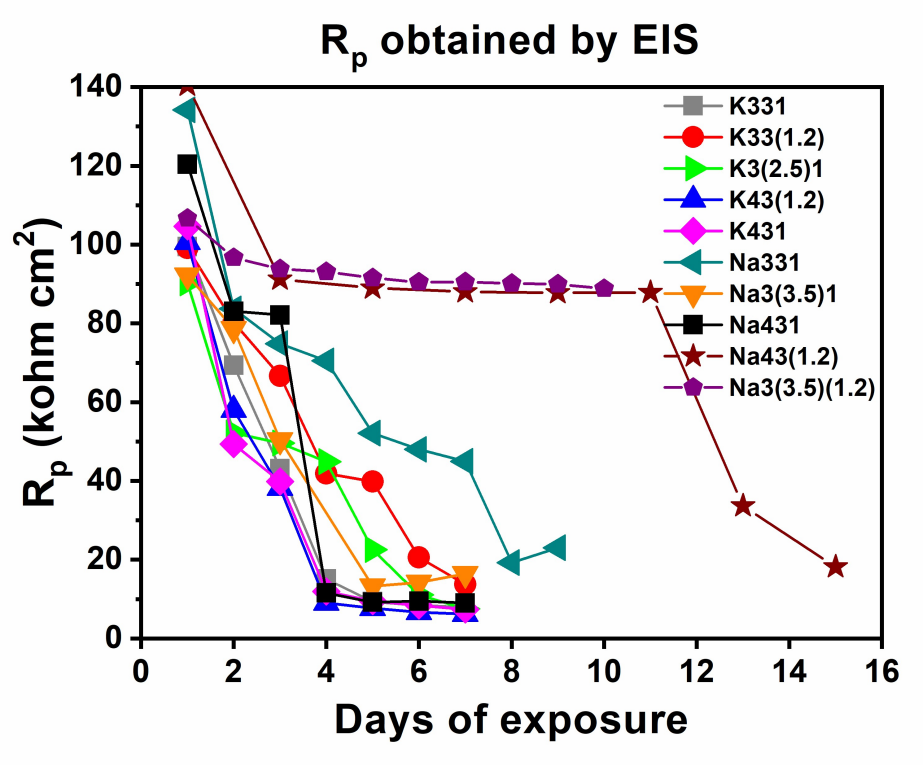

Figure 20. Polarization resistance of the GPCs for immersion tests.

Compared to the K-based GPC samples, the Na-based GPC samples showed a relatively better barrier performance, represented as the bigger polarization resistance values over a longer period of time. In case of the Na43(1.2), the polarization resistance is maintained at around 92 kohm-cm^2 range for around 10 days, which is in good agreement with the previous observation that in those samples, electrolyte gradually penetrated during the couple initial days, then delayed by the inner part of the concrete matrix, so the charge-transfer resistance of the steel rebar itself could be well-maintained until the electrolyte fully penetrates the concrete matrix. Compared to the K-based GPC that entered the free corroding range in the early period of immersion, the Na-based samples, especially Na43(1.2) entered such zone at much delayed immersion period, at around 15 days of immersion.

Meanwhile, compared to the K-based GPC samples, the Na-based GPC samples also revealed the sudden drop of the polarization resistance similar to OCP results. As the rebar faces the electrolyte with high chloride ion concentration without any relieved chloride filters, the charge-transfer resistance of the working electrode, rebar, decreased considerable in a short period of time, which resulted in such an abrupt decrease of the polarization resistance at last.

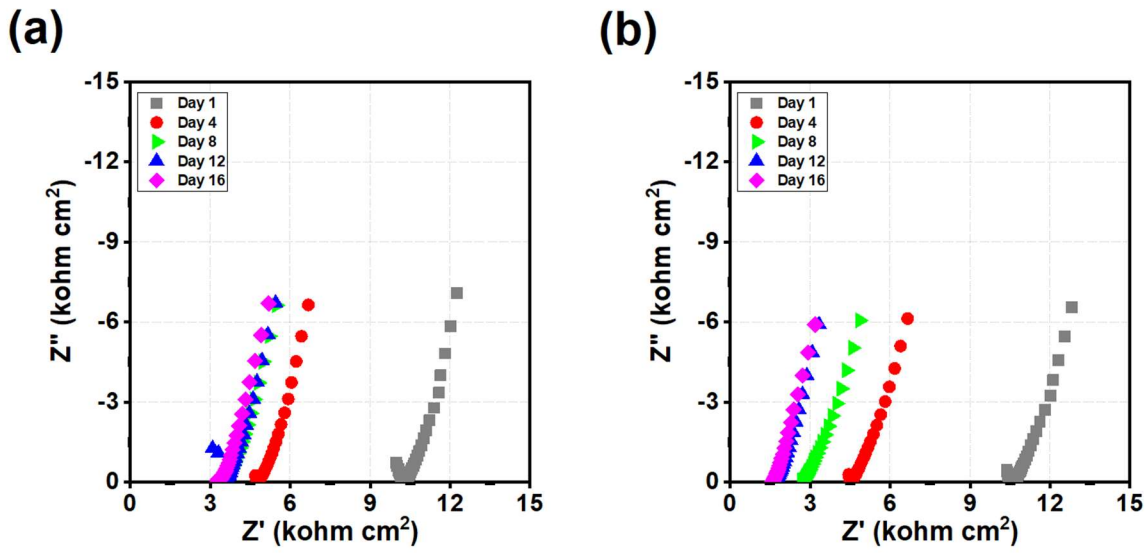

Figure 221. Nyquist plot of (a) K3(2.5)(1.2) and (b) K33(1.2) under fog chamber testing.

According to the Figure 21 that shows the Nyquist plot of the potassium-based GPCs, it is observable that the reinforcing bar has maintained its resistance up until the 16th day of the testing. This is possibly indicative of that the water uptake can be accelerated by the dam-type set up during the immersion which can provide the hydraulic pressure. As the fog chamber operation forms only a thin water layer at the entrance of the GPC sample with almost negligible pressure toward to the reinforcing bar, it may occur delayed water uptake throughout the concrete matrix.

5.5. Materials Characterization

5.5.1. X-ray Diffraction

As it can observed in Figure , a significant number of needle-shaped crystals grew on the surface of all the K-based GPC samples. It was an interesting phenomenon, and it was hypothesized to be either NaCl or KCl since the GPC is K-based and the electrolyte solution contains NaCl. It should also be pointed out that the two K-GP compositions that performed better than the rest, namely K3(2.5)1 and K33(1.2) had less surface crystals than the rest of the K-GP compositions by the end of the testing. It could be hypothesized that the growth of the crystals indicates the severe corrosion of rebar.

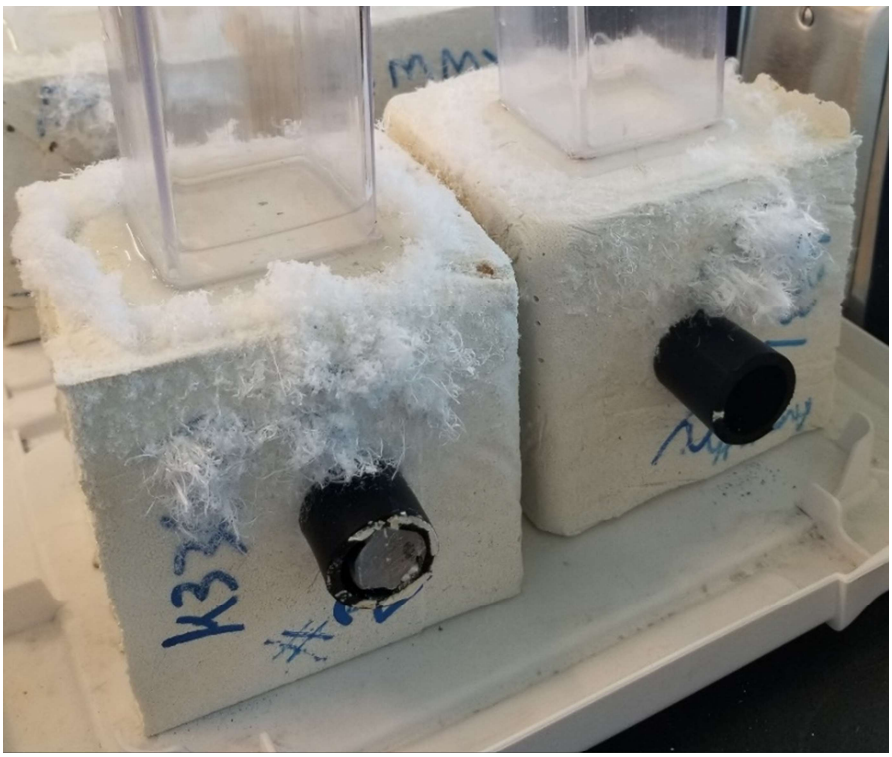

Figure 22. K-GPC after electrochemical test.

Figure shows the experimental XRD spectrum of the K-GPC surface crystals, and when it is cross-checked with the theoretical spectra of the hypothesized chloride compounds in Figure (*60*), it can be clearly see that the surface crystals are KCl. This is a very interesting finding since it shows that the potassium in the GPC is actually trapping the chloride ions, and then the sodium exchanges place with potassium and stays in the GP matrix.

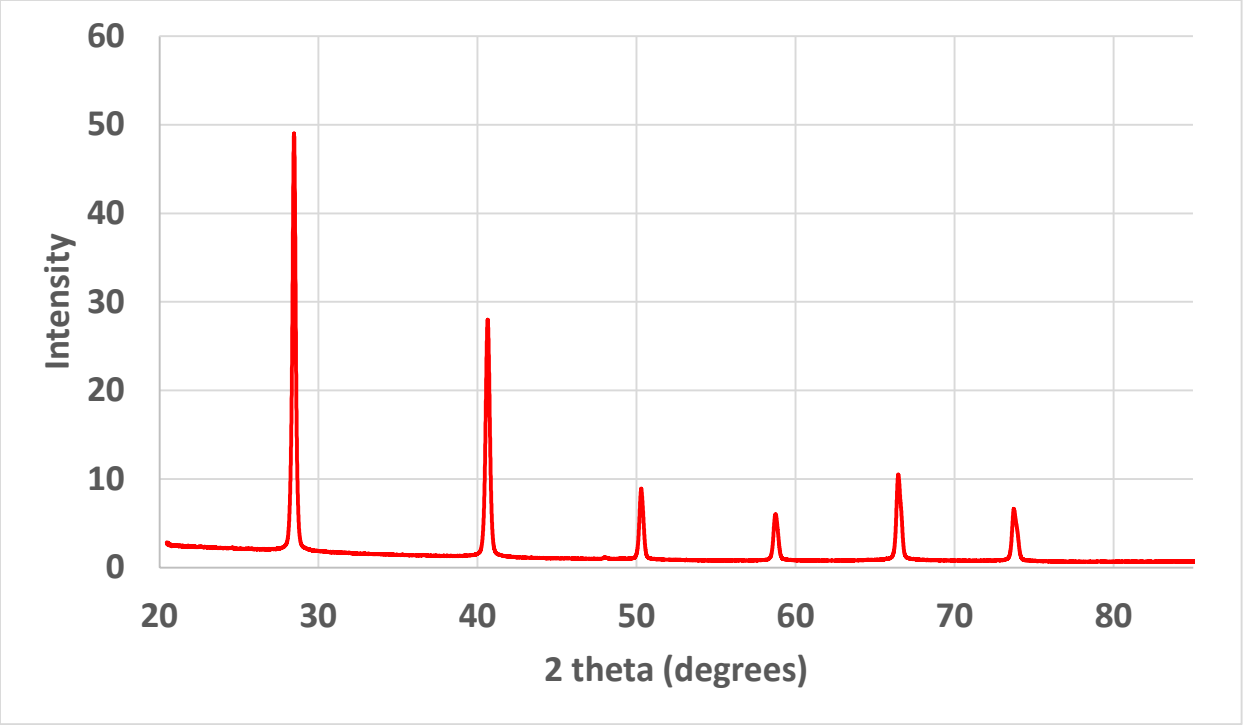

Figure 23. Experimental XRD Spectrum of K-GPC Surface Crystals.

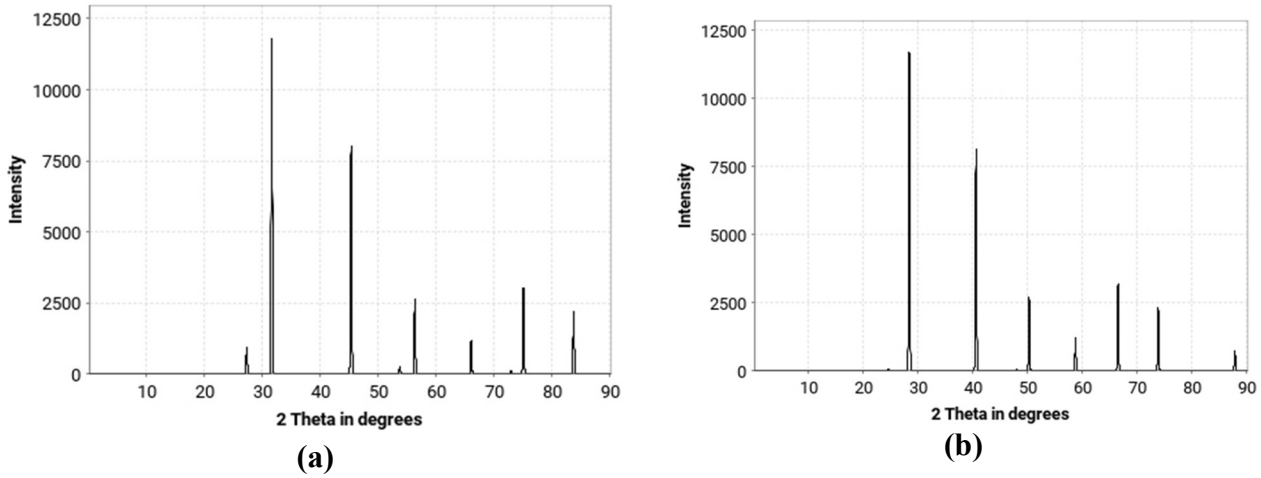

Figure 24. Theoretical XRD Spectra of (a) NaCl and (b) KCl from ICSD.

5.5.2. Optical Microscopy

Figure shows the optical microscopy images on the cross-sectional view of K331 and K33(1.2) in the region close to the rebar after immersion tests. It is important to note that there seems to be a significant amount of corrosion product forming on interface of the rebar and within the GPC matrix. This could potentially be an indication that GPC is absorbing the dissolved iron, which could potentially be a beneficial mechanism that prevents the formation of cracking and spalling of the concrete. However, this would need to be further investigated through SEM-EDS and longer testing period.

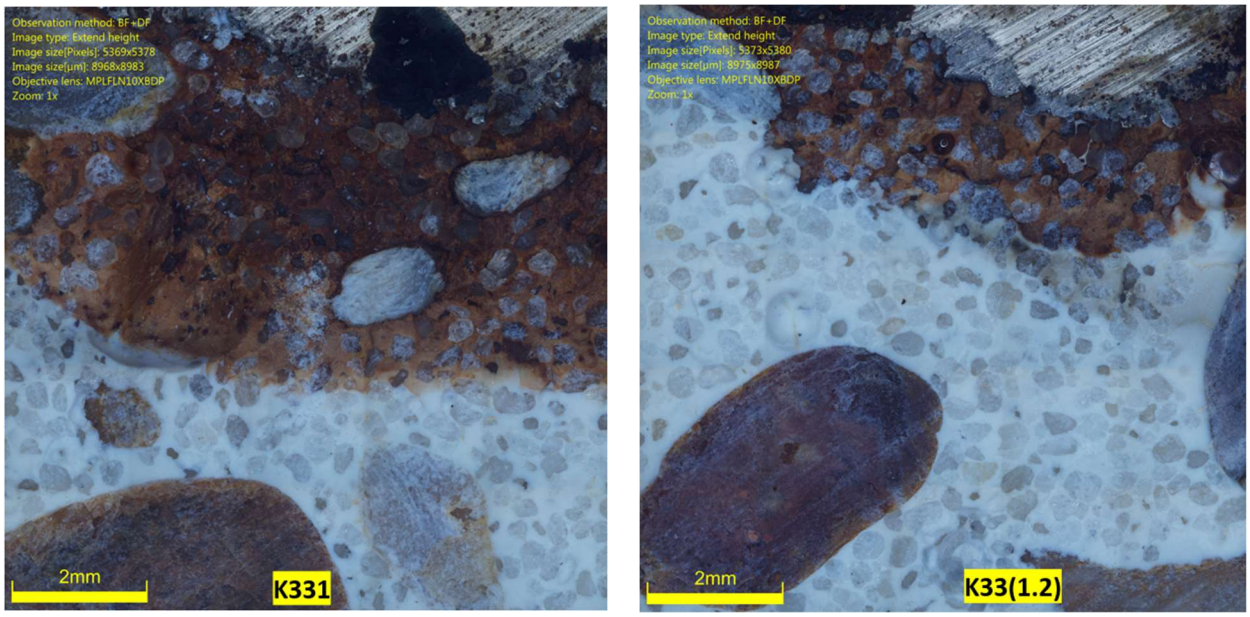

(a) **(b)**

Figure 25. Optical Microscopy of (a) K331 and (b) K33(1.2) from Set 1.

6. CONCLUSIONS

Durability of reinforced Geopolymer-based Concrete in corrosive environment has been characterized with promising results from the mass transport process mechanism or physical barrier blocking mechanism.

The electrochemical results suggest physical barrier mechanism blocking the chloride when the GPC materials are formed, where the mass transport process dominates and the physical results.

Overall, Na-based geopolymer shows a much better resistance of chloride-induced rebar corrosion than K-based geopolymer. However, K-based geopolymer seems to allow the rebar to corrode gradually, which is more ideal when compared to Na-based GP, which goes from no corrosion to severe corrosion within a day.

Out of all the compositions, Na43(1.2) and Na3(3.5)(1.2) have significantly outperforms the rest of the tested compositions. It's important to keep in mind that these are not the most optimal compositions, but from the result of this study, it can be concluded that SiO_2/Al_2O_3 ratio of 3 outperforms 4, and lower water/solids ratio and high alkali/Al ratio produces geopolymer-based cement with better resistance to rebar corrosion.

The growth of surface crystal (in the case of K-GPC, it's KCl) could be an indication of severe corrosion of the rebar.

Optical microscopy showed a relatively dense concrete matrix after immersion test. Even though the electrochemical has indicated severe corrosion in the rebar, the interface between GPC binder and rebar still seems to be preserved.

There is a second potential mechanism that can be used as a synergetic process to enhance the corrosion resistance property.

REFERENCES

1. Mehta, P. K., and P. J. Monteiro. *Concrete microstructure, properties and materials*. McGraw-Hill Education, 2017.
2. Goldsberry, R., J. Milla, M. McElwee, M. M. Hassan, and H. Castaneda. Evaluation of Microencapsulated Corrosion Inhibitors in Reinforced Concrete.In *International Congress on Polymers in Concrete*, Springer, 2018: 99-105.
3. Goldsberry, R. K. Electrochemical Evaluation of Self-Healing Epoxy Coated Rebar in Simulated Concrete Pore Solution.In *Materials Science & Engineering*, Texas A&M University, College Station, TX, 2019. Master of Science.
4. Popov, B. N. *Corrosion engineering: principles and solved problems*. Elsevier, 2015.
5. Lee, H., and D. Hiam. Corrosion resistance of galvannealed steel. *Corrosion,* 1989. 45, 10: 852-856.
6. Gartner, E. Industrially interesting approaches to "low-CO2" cements. *Cement and Concrete Research,* 2004. 34, 9: 1489-1498.
7. Mindess, S., J. F. Young, and D. Darwin. *Concrete*. 2003.
8. Shayan, A. Specification and use of geopolymer concrete in the manufacture of structural and non-structural components: review of literature.In, 2016.
9. Provis, J. L., and J. S. J. Van Deventer. *Geopolymers: structures, processing, properties and industrial applications*. Elsevier, 2009.
10. Xu, H., and J. S. Van Deventer. Geopolymerisation of multiple minerals. *Minerals Engineering,* 2002. 15, 12: 1131-1139.
11. Cheng, T.-W., and J. Chiu. Fire-resistant geopolymer produced by granulated blast furnace slag. *Minerals Engineering,* 2003. 16, 3: 205-210.
12. Hardjito, D., S. E. Wallah, D. M. Sumajouw, and B. V. Rangan. On the development of fly ash-based geopolymer concrete. *Materials Journal,* 2004. 101, 6: 467-472.
13. McLellan, B. C., R. P. Williams, J. Lay, A. Van Riessen, and G. D. Corder. Costs and carbon emissions for geopolymer pastes in comparison to ordinary portland cement. *Journal of Cleaner Production,* 2011. 19, 9-10: 1080-1090.
14. Davidovits, J. Geopolymers: inorganic polymeric new materials. *Journal of Thermal Analysis Calorimetry,* 1991. 37, 8: 1633-1656.
15. Davidovits, J. Geopolymers: Ceramic-like inorganic polymers. *J. Ceram. Sci. Technol,* 2017. 8, 3: 335-350.
16. Lyon, R. E., P. Balaguru, A. Foden, U. Sorathia, J. Davidovits, and M. Davidovics. Fire-resistant aluminosilicate composites. *Fire and materials,* 1997. 21, 2: 67-73.
17. Van Jaarsveld, J., J. Van Deventer, and A. Schwartzman. The potential use of geopolymeric materials to immobilise toxic metals: Part II. Material and leaching characteristics. *Mineral Engineering,* 1999. 12, 1: 75-91.
18. Papa, E., M. Mor, A. N. Murri, E. Landi, and V. Medri. Ice-templated geopolymer beads for dye removal. *Journal of Colloid and Interface Science,* 2020.
19. Duxson, P., S. W. Mallicoat, G. C. Lukey, W. M. Kriven, and J. S. van Deventer. The effect of alkali and Si/Al ratio on the development of mechanical properties of metakaolin-based geopolymers. *Colloids and Surfaces A: Physicochemical and Engineering Aspects,* 2007. 292, 1: 8-20.
20. Detphan, S., and P. Chindaprasirt. Preparation of fly ash and rice husk ash geopolymer. *International Journal of Minerals, Metallurgy and Materials,* 2009. 16, 6: 720-726.

21. Tchakoute, H. K., A. Elimbi, B. D. Kenne, J. Mbey, and D. Njopwouo. Synthesis of geopolymers from volcanic ash via the alkaline fusion method: effect of Al2O3/Na2O molar ratio of soda–volcanic ash. *Ceramics International,* 2013. 39, 1: 269-276.
22. Duxson, P., A. Fernández-Jiménez, J. L. Provis, G. C. Lukey, A. Palomo, and J. S. J. Van Deventer. Geopolymer technology: The current state of the art. *Journal of Materials Science,* 2007. 42: 2917-2933.
23. Duxson, P., J. L. Provis, G. C. Lukey, F. Separovic, and J. S. van Deventer. 29Si NMR study of structural ordering in aluminosilicate geopolymer gels. *Langmuir,* 2005. 21, 7: 3028-3036.
24. Palomo, A., A. Fernández-Jiménez, and M. Criado. "Geopolymers": same basic chemistry, different microstructures. *Materiales de Construccion,* 2004. 54, 275: 77-91.
25. Lizcano, M., A. Gonzalez, S. Basu, K. Lozano, and M. Radovic. Effects of water content and chemical composition on structural properties of alkaline activated metakaolin-based geopolymers.In *Journal of the American Ceramic Society*, 2012. 95: 2169-2177.
26. Davidovits, J. *Geopolymer, green chemistry and sustainable development solutions: proceedings of the world congress geopolymer 2005*. Geopolymer Institute, 2005.
27. Xu, H., and J. S. Van Deventer. Effect of source materials on geopolymerization. *Industrial & Engineering Chemistry Research,* 2003. 42, 8: 1698-1706.
28. Lizcano, M., H. S. Kim, S. Basu, and M. Radovic. Mechanical properties of sodium and potassium activated metakaolin-based geopolymers. *Journal of Materials Science,* 2012. 47: 2607-2616.
29. Hardjito, D., S. E. Wallah, D. M. J. Sumajouw, and B. V. Rangan. Factors Influencing the Compressive Strength of Fly Ash-Based Geopolymer Concrete. *Civil Engineering Dimension,* 2004. 6: pp. 88-93.
30. Hardjito, D., S. Wallah, D. Sumajouw, and B. Rangan. Introducing fly ash-based geopolymer concrete: manufacture and engineering properties.In *30th conference on our world in concrete & structures*, 2005: 23-24.
31. Duxson, P., G. C. Lukey, and J. S. J. van Deventer. Physical evolution of Na-geopolymer derived from metakaolin up to 1000 °C. *Journal of Materials Science,* 2007. 42: 3044-3054.
32. Mo, B.-h., H. Zhu, X.-m. Cui, Y. He, and S.-y. Gong. Effect of curing temperature on geopolymerization of metakaolin-based geopolymers. *Applied Clay Science,* 2014. 99: 144-148.
33. White, C. E., J. L. Provis, T. Proffen, and J. S. Van Deventer. The effects of temperature on the local structure of metakaolin-based geopolymer binder: A neutron pair distribution function investigation. *Journal of the American Ceramic Society,* 2010. 93, 10: 3486-3492.
34. Zhang, B., K. J. MacKenzie, and I. W. Brown. Crystalline phase formation in metakaolinite geopolymers activated with NaOH and sodium silicate. *Journal of Materials Science,* 2009. 44, 17: 4668-4676.
35. Bell, J. L., P. E. Driemeyer, and W. M. Kriven. Formation of ceramics from metakaolin-based geopolymers. Part II: K-based geopolymer. *Journal of the American Ceramic Society,* 2009. 92, 3: 607-615.
36. Rowles, M., and B. O'Connor. Chemical optimisation of the compressive strength of aluminosilicate geopolymers synthesised by sodium silicate activation of metakaolinite. *Journal of Materials Chemistry,* 2003. 13, 5: 1161-1165.
37. Zhang, M., M. Zhao, G. Zhang, T. El-Korchi, and M. Tao. A multiscale investigation of reaction kinetics, phase formation, and mechanical properties of metakaolin geopolymers. *Cement and Concrete Composites,* 2017. 78: 21-32.

38. Subaer, and A. van Riessen. Thermo-mechanical and microstructural characterisation of sodium-poly(sialate-siloxo) (Na-PSS) geopolymers. *Journal of Materials Science,* 2007. 42, 9: 3117-3123.
39. Marín-López, C., J. L. Reyes Araiza, A. Manzano-Ramírez, J. C. Rubio Avalos, J. J. Perez-Bueno, M. S. Muñiz-Villareal, E. Ventura-Ramos, and Y. Vorobiev. Synthesis and characterization of a concrete based on metakaolin geopolymer. *Inorganic Materials,* 2009. 45, 12: 1429-1432.
40. Olivia, M., and H. Nikraz. Properties of fly ash geopolymer concrete designed by Taguchi method. *Materials & Design (1980-2015),* 2012. 36: 191-198.
41. Škvára, F., V. Šmilauer, P. Hlaváček, L. Kopecký, and Z. Cílová. A weak alkali bond in (N, K)-A-S-H gels: Evidence from leaching and modeling. *Ceramics - Silikaty,* 2012. 56: 374-382.
42. Miranda, J. M., A. Fernández-Jiménez, J. A. González, and A. Palomo. Corrosion resistance in activated fly ash mortars. *Cement and Concrete Research,* 2005. 35: 1210-1217.
43. Reddy, D. V., J.-B. Edouard, and K. Sobhan. Durability of Fly Ash–Based Geopolymer Structural Concrete in the Marine Environment. *Journal of Materials in Civil Engineering,* 2013. 25: 781-787.
44. Shaikh, F. U. A. Effects of alkali solutions on corrosion durability of geopolymer concrete. 2014. 2: 109-123.
45. Chindaprasirt, P., and W. Chalee. Effect of sodium hydroxide concentration on chloride penetration and steel corrosion of fly ash-based geopolymer concrete under marine site. *Construction and Building Materials,* 2014. 63: 303-310.
46. Babaee, M., and A. Castel. Chloride-induced corrosion of reinforcement in low-calcium fly ash-based geopolymer concrete. *Cement and Concrete Research,* 2016. 88: 96-107.
47. Tennakoon, C., A. Shayan, J. G. Sanjayan, and A. Xu. Chloride ingress and steel corrosion in geopolymer concrete based on long term tests. *Materials & Design,* 2017. 116: 287-299.
48. Gunasekara, C., D. Law, S. Bhuiyan, S. Setunge, and L. Ward. Chloride induced corrosion in different fly ash based geopolymer concretes. *Construction and Building Materials,* 2019. 200: 502-513.
49. Zhang, R., A. Castel, and R. François. Influence of steel–concrete interface defects owing to the top-bar effect on the chloride-induced corrosion of reinforcement. *Magazine of concrete research,* 2011. 63, 10: 773-781.
50. ASTM. Standard Specification for Standard Sand.In, ASTM International, West Conshohocken, PA, 2017. C778-17.
51. Cho, S., T.-M. Chiu, and H. Castaneda. Electrical and electrochemical behavior of a zinc-rich epoxy coating system with carbon nanotubes as a diode-like material. *Electrochimica Acta,* 2019. 316: 189-201.
52. Kim, C., A. I. Karayan, J. Milla, M. Hassan, and H. Castaneda. Smart Coating Embedded with pH-Responsive Nanocapsules Containing a Corrosion Inhibiting Agent. *ACS Applied Materials & Interfaces,* 2020. 12, 5: 6451-6459.
53. Castaneda, H., M. Hassan, M. Radovic, and J. Milla. Self-Healing Microcapsules as Concrete Aggregates for Corrosion Inhibition in Reinforced Concrete. 2018.
54. Aneja, K. S., S. Bohm, A. Khanna, and H. M. Bohm. Graphene based anticorrosive coatings for Cr (VI) replacement. *Nanoscale,* 2015. 7, 42: 17879-17888.
55. Suay, J., M. Rodriguez, R. Izquierdo, A. Kudama, and J. Saura. Rapid assessment of automotive epoxy primers by electrochemical techniques. *Journal of Coatings Technology,* 2003. 75, 945: 103-111.

56. Bertolini, L., B. Elsener, P. Pedeferri, E. Redaelli, and R. Polder. *Corrosion of steel in concrete*. Wiley Online Library, 2013.
57. Ford, S., J. Shane, and T. O. Mason. Assignment of features in impedance spectra of the cement-paste/steel system. *Cement and Concrete Research,* 1998. 28, 12: 1737-1751.
58. Hirschorn, B., M. E. Orazem, B. Tribollet, V. Vivier, I. Frateur, and M. Musiani. Constant-phase-element behavior caused by resistivity distributions in films: I. Theory. *Journal of The Electrochemical Society,* 2010. 157, 12: C452.
59. Hsu, C., and F. Mansfeld. Concerning the conversion of the constant phase element parameter Y0 into a capacitance. *Corrosion,* 2001. 57, 9: 747-748.
60. Cherginets, V. L., V. N. Baumer, S. S. Galkin, L. V. Glushkova, T. P. Rebrova, and Z. V. Shtitelman. Solubility of Al2O3 in Some Chloride− Fluoride Melts. *Inorganic chemistry,* 2006. 45, 18: 7367-7371.

61. Kim, C., Cho, S., Yang, W., A. I. Karayan, and H. Castaneda. Corrosion Behavior of Al-Si-Mg Coated Hot-Press-Forming Steel. Corrosion Science, 2021. 183: 109339.